1971

Final sintering of Cr_2O_3 with minor additions of MgO and sintering of MgO with minor additions of Cr_2O_3

Gordon E. Jungquist

Department:

FINAL SINTERING OF Cr_2O_3 WITH MINOR ADDITIONS OF MgO AND SINTERING OF MgO WITH MINOR ADDITIONS OF Cr_2O_3

BY

GORDON ERIC JUNGQUIST, 1946-

A

THESIS

Presented to the Faculty of the Graduate School of the

UNIVERSITY OF MISSOURI-ROLLA

In Partial Fulfillment of the Requirements for the Degree

MASTER OF SCIENCE IN CERAMIC ENGINEERING

1971

Approved by

P. Darrell Crowley (Advisor) William A. Isaac

Robert E. Moore

ABSTRACT

The effect of oxygen activity on the sintering of Cr_2O_3 with minor additions of MgO, and of MgO with minor additions of Cr_2O_3 at 1600°C was investigated. A peak density (99.4% of theoretical) was obtained for high purity Cr_2O_3 by maintaining the equilibrium oxygen partial pressure needed to maintain the Cr_2O_3 phase. The addition of 0.1 wt. % MgO increased the sintered density at the same oxygen pressure to 99.8%. Further MgO additions decreased the density. The density of pure MgO was independent of the P_{O_2} over the range investigated. Addition of Cr_2O_3 to MgO decreased the density at all oxygen pressures investigated. The largest decreases corresponded to the pressure ranges where the most volatile species in the Cr-O system appear.

The weight loss was also monitored as a function of oxygen activity for all specimens. It was found to correlate with the changing predominant volatile species in the chrome-oxygen system. An anomalous weight loss of MgO was found at $P_{O_2} \leq 10^{-12}$ atm which may be due to a volatile Mg-Cr oxide species.

ACKNOWLEDGEMENTS

The author expresses his appreciation for the encouragement and guidance of his advisor, Dr. P. Darrell Ownby. Appreciation is also expressed to Dr. Harlan Anderson for his helpful comments and assistance.

The author wishes to thank the American Iron and Steel Institute for financial support during the course of this investigation.

TABLE OF CONTENTS

Page

LIST OF ILLUSTRATIONS

LIST OF ILLUSTRATIONS (Cont.)

Figures Page

LIST OF TABLES

I. INTRODUCTION

The objective of this research was to determine the relative effect of minor additions of Cr_2O_3 to MgO and of MgO to Cr_2O_3 on the sintering of the two oxides. The sintering was performed under different controlled atmospheres to determine if atmospheric conditions altered the effect of the minor additions.

These two materials, MgO and Cr_2O_3, are the two major components of magnesite-chrome refractories. It is known that the major causes for deterioration of these refractories is impurity uptake due to low purity and low density. Since the magnesite-chrome refractories themselves present a very complex system to study with many uncontrollable variables, a direct investigation of the densification of the complete refractory composition with all of the impurity constituents and uncontrollable variables was not attempted. Rather, this investigation consists of a study of the densification of the pure major components of the magnesite-chrome system (MgO and Cr_2O_3) and the effect of the two components on one another during sintering. By using this approach a better understanding of some of the important basic variables involved in the mass transport mechanisms which lead to densification in magnesite-chrome refractories can be gained.

It has been established[1,2], that minor second oxide additions to a main oxide component can, in many cases, aid

in sintering to theoretical density. In other systems a second oxide can be very detrimental to sintering[2,3]. The effect of even very small additions of one component on another is very important.

The atmospheric conditions are also significant factors in sintering. They affect the defect structure, the oxidation state of the metal ions, and the chemical phases present. In addition different gases diffuse out of closed pores in sintered powder compacts at different rates. All these factors must be considered in even simple binary systems when sintering to high densities.

II. REVIEW OF LITERATURE

A. Effects of Minor Additives

The minor addition of a solute to an oxide can cause one of four results as indicated by Jorgensen[1]: "(1) modify the defect structure of the solvent, (2) form a liquid phase, (3) form a solid second phase which pins boundaries, or (4) segregate at grain boundaries reducing boundary mobility." Since sintering kinetics are determined by diffusion mechanisms, if an additive modifies the defect structure and increases the solid state diffusion coefficients of the rate limiting species, then acceleration of the sintering kinetics will be observed. The presence of a liquid phase usually speeds up sintering kinetics due to greater diffusion coefficients. Sintering kinetics can also be enhanced by maintaining small grains. This minimizes the distance for vacancy diffusion from the pores to the grain boundaries which act as vacancy sinks. The difference between mechanisms (1) and (3) or (4) is that a solute that alters the diffusion coefficients influences all stages of sintering. A solute that prevents grain growth, however, influences only the latter stages of sintering.

Several studies have been conducted on the role of minor additions of Cr_2O_3 on the sintering of MgO. Nelson and Cutler[2] studied the effects of oxides (including Cr_2O_3) on the sintering of MgO in air. The MgO was obtained from calcined magnesium carbonate (analytical reagent grade).

Their results, shown in Table I, indicated that MgO decreased in sintered density with increase in addition of Cr_2O_3 at 1400° and 1600°C. The amounts of additions of Cr_2O_3 were 0.5 mole % (1.8 wt. %) and higher. The addition of 0.5 mole % Cr_2O_3 at 1600°C showed no change in % theoretical density from that of MgO without an additive. They hypothesized that spinel formation was the cause of the decrease in sintered density.

Layden and McQuarrie[4] investigated the effect of minor additions to MgO. Their results (Table I) indicated that up to 0.1 atomic % Cr ions (0.1 mole % Cr $(NO_3)_3 \cdot 9H_2O$ addition to magnesium carbonate) can go into solid solution in MgO and aid sintering at 1225°C. Higher concentrations and higher temperatures decrease the density significantly. Above this solubility limit, the excess forms spinel and hinders sintering. They supported this view by their observation of the color of the specimens. The ones with 0.1 atomic % were buff in color indicating the Cr ion was free to assume its normal low temperature valence state (6+). The others were a green color indicating the Cr ion had assumed its high temperature valence state (3+) which was stabilized in the form of a compound.

In another investigation on the effect of minor additions of Cr_2O_3 to MgO, Hench and Russell[3] presented evidence that MgO decreased in sintered density with increase in addition of Cr_2O_3 at 2,600°F (1427°C) and 2,400°F (1317°C). They indicated that in air at the

TABLE I

Literature Review of MgO+X Percent Cr_2O_3

% Theoretical Density of MgO

Nelson and Cutler				Layden and McQuarrie			
Mole %	Wt.%*	1400°C	1600°C	Mole %	Wt.%*	1225°C	1525°C
0.0	0.0	88.0	96.0	0	0	60.5	89.5
0.5	1.86	58.0	96.5	0.05	0.19	74.0	86.5
1.0	3.66	57.0	93.0	0.25	0.94	46.2	72.5
2.0	7.06	52.0	83.0	0.5	1.86	37.7	86.5
4.0	13.19	55.0	70.0				
8.5	24.41	53.0	71.0				

Hench		
Mole %*	Wt. %	2600°F (1427°C)
0.0	0.0	94.0
0.05	0.19	88.0
0.13	0.5	75.5
0.26	1.0	63.1
0.53	2.0	58.4
0.81	3.0	54.0
1.36	5.0	52.6
2.84	10.0	45.6

* Calculated by the author of this paper

firing temperatures CrO_3 volatilized and then reacted with the MgO to form a spinel layer around the MgO grains. They also stated that the spinel layer hindered diffusion of the MgO to neck regions between particles and, thus, retarded further sintering.

Due to the high volatilization in oxidizing atmospheres, little work has been done on the sintering of Cr_2O_3. There has not been any work published on the effect of MgO additions to Cr_2O_3. Caplan and Cohen[6] studied the volatilization of Cr_2O_3. They showed that Cr_2O_3 oxidizes to form gaseous CrO_3 in oxygen at 1200°C. They also indicated moisture accelerated the reaction. Hagel and Seybolt[7] investigated the cation diffusion in Cr_2O_3 and Hagel[8] investigated the anion diffusion in Cr_2O_3. A comparison indicated that the anion was the slower diffusing ion at 1450°C by a factor of $10^{-4}cm^2/sec$ (diffusion coefficients were $Cr \sim 10^{-8}cm^2/sec$ and $O \sim 10^{-12}cm^2/sec$). Hagel, Jorgensen and Tomalin[9] studied the initial sintering of Cr_2O_3. Because of the high volatilization in an oxidizing atmosphere, an argon atmosphere with a P_{O_2} of about 10^{-2} atm was maintained. Their work indicated that Cr_2O_3 sintered by the volume-diffusion process where the oxygen ion was rate controlling.

Hench[5] also studied the sintering of Cr_2O_3, however his investigation was conducted in air. He indicated that both evaporation-condensation and volume diffusion

mechanisms were taking place. The evaporation-condensation occurred at a higher rate than the volume diffusion. Since the evaporation-condensation mechanism doesn't result in shrinkage, little shrinkage was observed. What little occurred was due to volume diffusion.

B. Atmospheric Effects on Sintering

Coble[10] has pointed out that atmospheric conditions during sintering can affect the rate of densification and the limiting density. The atmospheric conditions may affect the rate of densification by altering the defect structure in turn altering the diffusion rates of the diffusing species. For example, a change in oxygen pressure can change the number of oxygen vacancies in an oxide which affects the diffusion of the oxygen ions.

Coble also reviewed the effect of atmospheric conditions on the limiting density due to the diffusivity of the gas. Sealed pores containing a gas with the lowest diffusivity imaginable in a compact will shrink to their stable size. After that the gas will not diffuse out of the pores. The large pores containing a gas with a slightly higher diffusivity will grow at the expense of the smaller pores. These specimens will bloat after reaching maximum density. Pores will continue to shrink when a gas having a higher diffusivity is present. The shrinkage of the final pores is rate controlled by the kinetics of the gas diffusion to the surface. For very high gas diffusivi-

ties the final shrinkage of the specimen may be rate controlled by other densification mechanisms. It may depend chemically on the pressure and the species of the gas since these control the defect structure, the lattice diffusivities, and ultimately the sintering rate.

Coble studied the effect of atmospheres on the sintering of alumina with a small addition of MgO. He showed that hydrogen and oxygen permitted the alumina to sinter to theoretical density. However, air, nitrogen, helium, and argon impeded the sintering of alumina to theoretical density. He attributed this to the insolubility of the latter group of gases in alumina.

Jones, Maitra, and Cutler[11] studied the role of structural defects on the sintering of alumina and magnesia. This included firing in reducing (H_2), neutral (N_2), and oxidizing (O_2) atmospheres. Both Al_2O_3 and MgO showed no change in sintered density with change in atmosphere. The effect of minor additions of other oxides to Al_2O_3 and MgO in the same atmosphere was studied. The MgO with additions of 1 mole % TiO_2, ZrO_2 or Fe_2O_3 sintered to higher densities in an oxidizing or a neutral atmosphere. The Al_2O_3 samples with additions of Cr_2O_3 or Fe_2O_3 fired to higher densities in a reducing atmosphere, while Al_2O_3 with additions of MnO or TiO_2 sintered to higher densities in a neutral or an oxidizing atmosphere.

The type of firing atmosphere can also affect the chemical phases present. Hench and Russell[3] showed that the formation of CrO_3 vapor in the sintering of MgO with

additions of Cr_2O_3 in air led to a decrease in density of sintered MgO as mentioned in the previous section. From these observations the pronounced effects of atmospheric conditions on the sintering of oxides can be seen.

III. EXPERIMENTAL PROCEDURE

A. Materials

Fisher's Certified Magnesium Oxide* and Hyperrefiner's Ultra High Pure Chromium Oxide* were used as the main components in this study. The ultra high pure Cr_2O_3 was used as the additive to the MgO. Fisher's Certified Magnesium Nitrate* was used as the source of MgO additive to the Cr_2O_3.

Electronmicrographs of the MgO particles revealed the particle size to be less than 1 micron. The particles were in agglomerates between 1 and 5 microns in diameter. Electronmicrographs of the Cr_2O_3 particles also revealed them to be less than 1 micron. The Cr_2O_3 particles were in agglomerates 10 microns or larger, however.

The magnesium nitrate was used because it dissolves in water. This provided a better dispersion of the magnesium oxide in the chromium oxide compared to mixing of the two powders. Since smaller quantities of the MgO in the Cr_2O_3 was used than Cr_2O_3 in MgO, better dispersion of the MgO was required.

B. Fabrication of Samples

The small amounts of Cr_2O_3 were mixed with MgO in methanol. Water was not used to avoid the formation of $Mg(OH)_2$. Distilled water was used to mix the dissolved

---

* See Appendix A for a list of impurities.

magnesium nitrate with the Cr_2O_3. The mixtures were poured into a high speed blender and mixed for 10 minutes. This dispersed the minor additive in the main component and broke up agglomerates. The mixtures were then continuously stirred with a magnetic stirrer while the methanol or water was being evaporated on a hot plate. Final drying was done in a dryer over night. The powders were then forced through a 100 mesh seive to break up any agglomerates.

The Cr_2O_3 with magnesium nitrate was calcined for two hours at 600°C to decompose the magnesium nitrate to MgO.

After the mixtures were prepared, they were pressed into disks approximately 1/2" in diameter and 1/4" thick. They were first uniaxially pressed in a die with a hydraulic press at 10,000 psi to form them into the desired shape. This was followed by isostatic pressing at 30,000 psi. The isostatic pressing was done to insure a more uniform green density within the specimens. The MgO specimens pressed to 50-55% of theoretical density while the Cr_2O_3 samples pressed to 60-65% of theoretical density. (See Tables III, IV, and V).

Before firing the specimens, their diameter (d) thickness (L), and weight (W) were measured. These data were used to determine the green densities and % weight loss.

C. Controlled Atmospheres

Cr_2O_3 is readily oxidized to higher oxides which are highly volatile. These properties have been shown in the literature[5] to be very detrimental to the densification of Cr_2O_3 and MgO with additions of Cr_2O_3[2,5]. This systematic study of the effect of controlled atmospheres down to very low oxygen partial pressures was therefore made.

The partial pressure of oxygen was controlled using buffer systems to maintain the desired oxygen pressures over the unstable oxides. Two buffer systems were used during the course of the study, the hydrogen and water vapor and the CO_2 and CO systems. The equilibrium reaction for the H_2/H_2O buffer system is $2H_2O = 2H_2+O_2$. The equilibrium constant for this system is

$$K_{H_2/H_2O} = \frac{(P_{H_2})^2(P_{O_2})}{(P_{H_2O})^2}$$

The partial pressure of the oxygen was maintained by controlling the ratio of water vapor to hydrogen.

$$P_{O_2} = K_{H_2/H_2O}\left(\frac{P_{H_2O}}{P_{H_2}}\right)^2$$

The mixture of water vapor and hydrogen was obtained by bubbling 99.95% pure hydrogen through a flask of distilled water. The flask of water was submerged in a water bath (Figure 1) to maintain the distilled water to within

± 0.1°C of a specific temperature. It was assumed that the hydrogen bubbled through the water was saturated with the water vapor at that temperature. For lack of data on the amount of water vapor that will saturate H_2 at various temperatures, the values for air were taken realizing that the ratios of P_{H_2O}/P_{H_2} would only be relative and wouldn't represent exact values.

Because of this lack of accuracy and since water vapor has been noted to affect the grain growth of MgO, a second buffer system consisting of CO and CO_2 was used to maintain the P_{O_2}. The equilibrium reaction for this system is $2CO_2 = 2CO + O_2$. The equilibrium constant for this system is given by

$$K_{CO/CO_2} = \frac{(P_{CO})^2 (P_{O_2})}{(P_{CO_2})^2}$$

The partial pressure of the oxygen was maintained by controlling the ratio of P_{CO_2} to P_{CO}.

$$P_{O_2} = K_{CO/CO_2} \left(\frac{P_{CO_2}}{P_{CO}} \right)^2 \qquad (2)$$

The CO/CO_2 mixture was obtained by determining the flow rates of the two gases necessary to obtain the desired ratio. The gases were passed through a mixing chamber consisting of a glass tube filled with glass beads where they mixed prior to being passed into the furnace. In most cases the amount of CO_2 required was very low. Due

Figure 1. Mixing system for H_2/H_2O buffer system

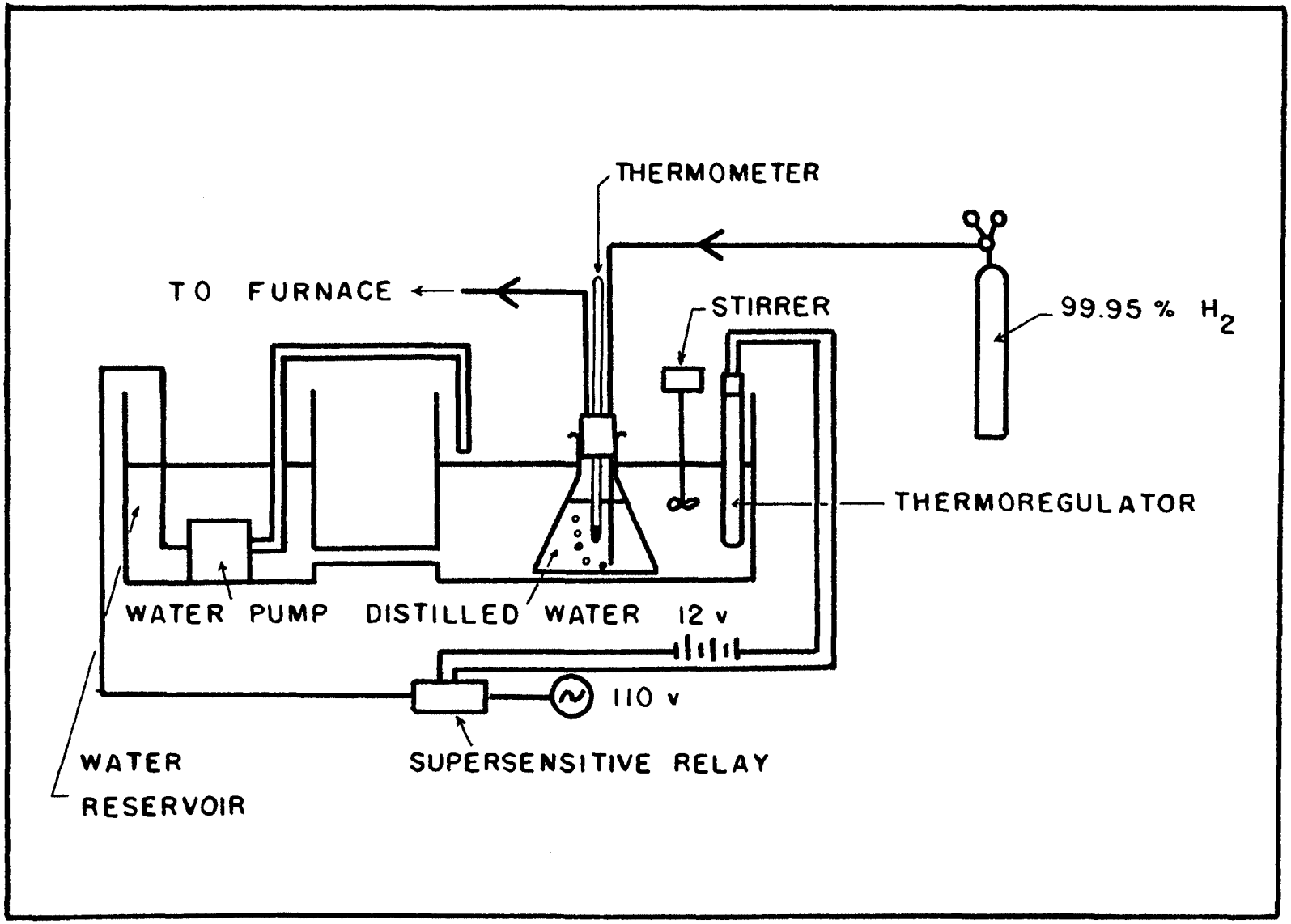
THERMOMETER
TO FURNACE
STIRRER
99.95 % H_2
THERMOREGULATOR
WATER PUMP
DISTILLED WATER
12 v
110 v
WATER RESERVOIR
SUPERSENSITIVE RELAY

Figure 1

to this difficulty, a mixed gas of N_2 with 5% CO_2 was used to introduce the CO_2. A couple of samples were fired in CO and CO_2 to verify that the P_{O_2} was the same as calculated whether or not the mixed gas was used. A combination of N_2 and O_2 was used to obtain a $P_{O_2} = 2 \times 10^{-2}$ atm. Air was used for a $P_{O_2} = 0.2$ atm and O_2 was used to obtain a $P_{O_2} = 1$ atm. A combination of N_2 and water vapor was used to observe any effect of water vapor on the sintering of MgO.

The free energy of formation for the two above mentioned reactions at 1600°C was obtained from the literature.[13] The $\Delta G°$ values for the two reactions at 1600°C are 68,000 cal/mole and 57,000 cal/mole respectively. The following equation was then used to obtain the P_{O_2} at equilibrium:

$$\Delta G° = -RT \ln P_{O_2} \qquad (3)$$

where $\Delta G°$ = free energy of formation

R = gas constant

T = temperature (°K)

If the ratio of P_{H_2O}/P_{H_2} or $P_{CO_2}/P_{CO} = 1$ at 1600°C, then the equilibrium constants in equations (1) and (2) will equal the P_{O_2} calculated from equation (3)

$$K_{H_2/H_2O} = P_{O_2}, \; K_{CO/CO_2} = P_{O_2}$$

The equilibrium constants were calculated to be 1.16×10^{-8} and 2.24×10^{-7} respectively. A list of the various partial pressures of oxygen and corresponding partial

pressure ratios of the two buffer systems appears in Table II.

Once the partial pressure ratios were calculated for each P_{O_2} using equations (1) and (2), the partial pressure of each species was calculated. Since the total pressure in the furnace was maintained at 1 atm, then according to Dalton's Law the sum of the partial pressures will equal 1 atm. Thus, for the H_2/H_2O buffer system:

$$P_T = 1 \text{ atm} = P_{H_2O} + P_{H_2} \tag{4}$$

and for the CO/CO_2 buffer system

$$P_T = 1 \text{ atm} = P_{CO_2} + P_{CO} + P_{N_2} \tag{5}$$

(From Amagat's Law and Boyle's Law the volume ratios and the partial pressure ratios are in the same proportion. Thus for N_2 with 5% CO_2, $V_{N_2} = 19V_{CO_2}$ and $P_{N_2} = 19P_{CO_2}$). Knowing the ratios of the various partial pressures of one gas to another, expressions (4) and (5) can be represented in terms of only one of the gaseous species and solved. For example:

$$\frac{P_{H_2O}}{P_{H_2}} = X$$

$$P_{H_2O} = XP_{H_2} \tag{6}$$

substituting (6) into (4)

$$P_T = 1 \text{ atm} = P_{H_2} + XP_{H_2}$$

TABLE II

Partial Pressures of Gases Used to Maintain P_{O_2}

P_{O_2}(atm)	P_{H_2}/P_{H_2O}	P_{H_2}(atm)	P_{H_2O}	P_{CO}/P_{CO_2}	P_{N_2}(atm)	P_{CO_2}(atm)	P_{CO}(atm)	$P_{N_2+CO_2}$(atm)
$9x10^{-14}$	--	--	--	1580/1	0.0114	0.0006	0.9880	0.0120
$9x10^{-13}$	--	--	--	464/1	0.0380	0.0020	0.9600	0.0400
$2x10^{-12}$	76.6/1	0.9872	0.0128atm	340/1	0.0513	0.0027	0.9460	0.0540
$6x10^{-12}$	--	--	--	252/1	0.0684	0.0036	0.9280	0.0720
$9x10^{-12}$	--	--	--	160/1	0.1045	0.0055	0.8900	0.1100
$2x10^{-11}$	24.2/1	0.9604	0.0396atm	100/1	0.1577	0.0083	0.8340	0.1660
$6x10^{-11}$	--	--	--	50.1/1	0.2698	0.0142	0.7160	0.2840
$2x10^{-10}$	7.66/1	0.8846	0.1154atm	31.6	0.3667	0.0193	0.6140	0.3860
$2x10^{-9}$	--	--	--	10/1	0.6327	0.0333	0.3340	0.6660
$2x10^{-8}$	--	--	--	3.55/1	0.8056	0.0424	0.1520	0.8480
$2x10^{-6}$	--	--	--	1/3.16	0.9348	0.0492	0.0160	0.9840
$2x10^{-4}$	--	--	--	1/31.6	0.9481	0.0499	0.0020	0.9980
$2x10^{-2}$	--	--	--	--	0.98	--	--	--
0.2(Air)	--	--	--		--	--	--	--
1 (O_2)	--	--	--	--	--	--	--	--
--	--	--	9.8mmHg	--	750.2mmHg	--	--	--
--	--	--	30.5mmHg	--	729.5mmHg	--	--	--
--	--	--	87.7mmHg	--	672.3mmHg	--	--	--

$$P_{H_2} = \frac{1 \text{ atm}}{1 + X} \qquad (7)$$

Then (7) can be substituted back into (6)

$$P_{H_2O} = XP_{H_2} = X\left(\frac{1 \text{ atm}}{1 + X}\right)$$

The P_{CO}, P_{CO_2} and P_{N_2} were calculated by the same method. An attempt was made to control the P_{H_2O}/P_{H_2} ratio by controlling the temperature of the water through which H_2 was bubbled as mentioned above. Control of the partial pressure ratios for the CO/CO_2 system was accomplished by controlling the flow rates of the CO and the N_2 + 5% CO_2.

The flow rate of each gas was calculated from the volume of gas required per second. It has been shown by Darken and Gurry[14] that a linear gas flow rate of 1 cm/sec is necessary to maintain equilibrium with the sample. Due to the design of the furnace tube, the flow rate was 7.12 cm^3/sec. Since the partial pressure ratios are in the same proportion as the volume ratios, the flow rates of CO and N_2 + CO_2 were calculated from the relationships

$$\frac{P_{CO}}{P_T} \cdot (7.12 \text{ cm}^3/\text{sec}) = \text{flow rate of CO}$$

$$\frac{P_{N_2} + P_{CO_2}}{P_T} \cdot (7.12 \text{ cm}^3/\text{sec}) = \text{flow rate of } N_2 + CO_2$$

D. Firing

A molybdenum wound tube furnace was used for firing the samples (Figure 2). The outside of the high purity

(99.8%) Al_2O_3 tube was encased in a stainless steel box. A stainless steel bellows was incorporated at one end of the furnace to allow for expansion of the Al_2O_3 tube. Silicone "O" rings were used to make gas tight seals between the stainless steel and the Al_2O_3 tube. Forming gas (N_2 + 10% H_2) was constantly passed through the casing to prevent oxidation of the molybdenum coil. Another high purity Al_2O_3 tube surrounded the furnace tube on the inside of the casing. This was done to keep the insulating bubbled Al_2O_3 from coming into contact with the molybdenum coil. A piece of Mo wire was strung through an Al_2O_3 rod the length of the outer Al_2O_3 tube. The wire was hooked at the ends of the outer Al_2O_3 tube. Hooks of Mo wire were hung on the Al_2O_3 rod. These hooks were used to suspend the Mo coil. This method prevented the Mo coil from coming into contact with the Al_2O_3 tube. Reaction between Mo and Al_2O_3 is known to be a major cause for failure of this type furnace. Two high current feedthroughs were used to connect the Mo wire to the power source and maintain a gas tight seal around the connection. A feedthrough was also used to connect a W-Re thermocouple with a temperature controller.

Aluminum end pieces were clamped on the ends of the furnace tube using silicone "O" rings to make a gas tight seal. Aluminum tubing extended from the end pieces for passing the gas through the inside of the furnace tube. A piece of glass was sealed over a 3/8" hole in one of the

Figure 2. Molybdenum wound tube furnace.

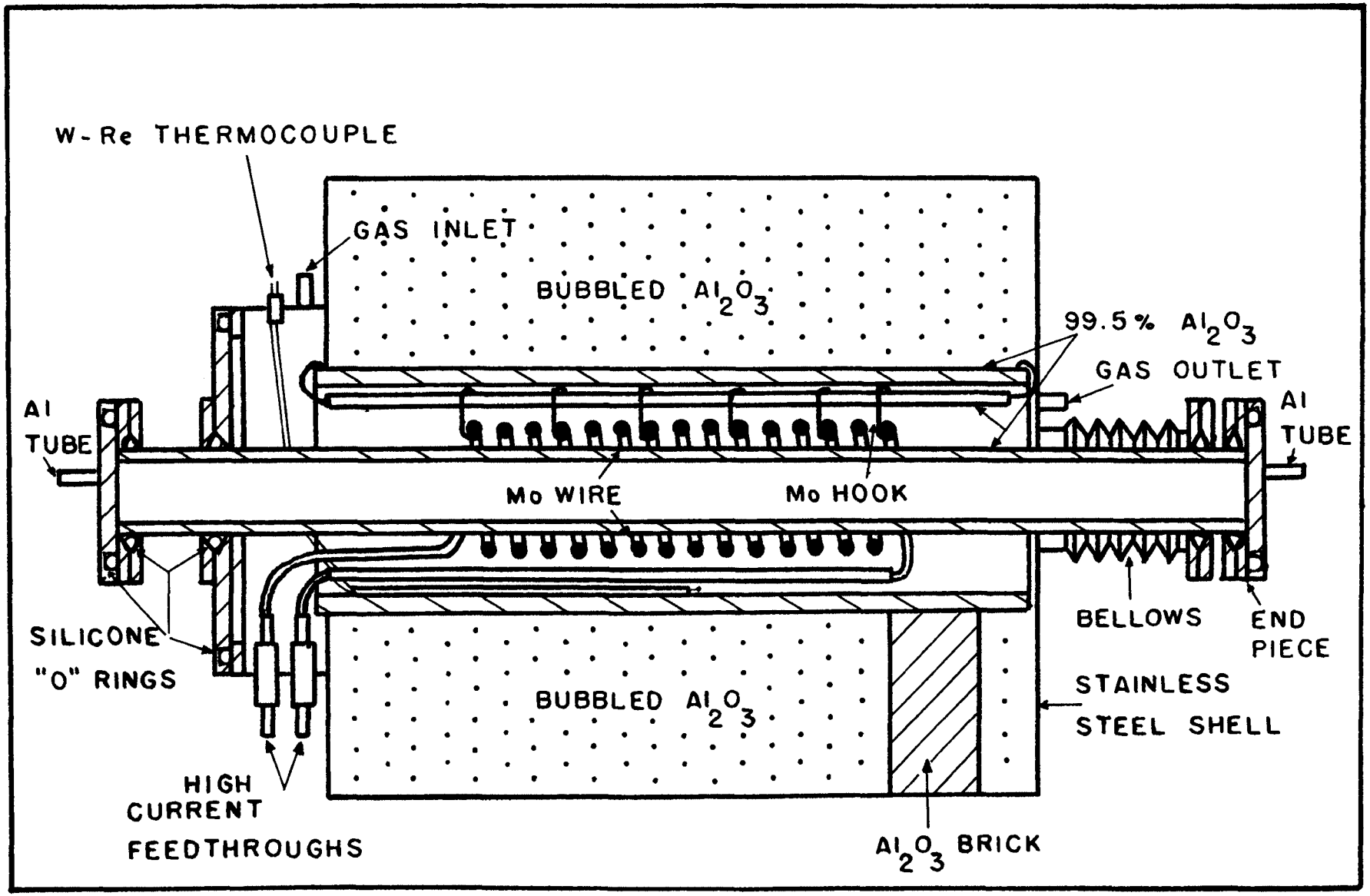
W-Re THERMOCOUPLE
GAS INLET
BUBBLED Al_2O_3
99.5% Al_2O_3
GAS OUTLET
Al TUBE
Al TUBE
Mo WIRE
Mo HOOK
SILICONE "O" RINGS
BELLOWS
END PIECE
BUBBLED Al_2O_3
STAINLESS STEEL SHELL
HIGH CURRENT FEEDTHROUGHS
Al_2O_3 BRICK

Figure 2

end pieces with silicone rubber for viewing into the furnace when sealed. Another hole with two silicone "O" rings was made at the same end as the viewing hole. This enabled an 18" long Al_2O_3 rod to slide through for introducing and withdrawing the samples from the hot zone while the atmospheric conditions were maintained.

The furnace was constantly maintained at 1600° ± 10°C. Samples were preheated to 800°C in another furnace. They were then slowly introduced into the hot zone to prevent thermal shock. The length of time a sample was sintered began when the sample reached the hot zone and stopped when it was removed from this region. The furnace tube was flushed 10 minutes with the gas to be used in the firing prior to introducing the sample into the hot zone.

E. Density Measurement

Once the specimens were fired, the relative effect of the additions and P_{O_2} was determined by measuring the bulk density of the specimens. Bulk density was measured by the xylene suspension and displacement method. A specimen was first weighed in air. It was then boiled in xylene for two hours. Its weight suspended in xylene was measured followed by its weight in air saturated with xylene. The following equation was used to calculate the bulk density:

$$B.D. = W_a/(W_{sat} - W_{sus})/D_x$$

B.D. = Bulk Density

W_a = weight in air

W_{sat} = weight saturated

W_{sus} = weight suspended

D_x = Density of xylene at room temperature

The precision of the bulk density measurements was ± 0.02 gm/cc. The bulk density was compared to the theoretical density of pure Cr_2O_3 (5.21 gm/cc) and of pure MgO (3.58 gm/cc) and expressed in percent of theoretical density.

F. Microstructure

The microstructure was examined by metallograph and scanning electron microscope. The polished sections were prepared by grinding on 240, 320, 400 and 600 grit SiC paper followed by polishing with one micron and 0.05 micron alumina powder. The MgO samples were etched with 50% solution of sulfuric acid. The Cr_2O_3 would not etch with acids so thermal etching was attempted with some success. They were heated to 1400°C for five minutes in air. The scanning electron microscope was used to examine the fractured surface of selected specimens.

IV. RESULTS AND DISCUSSION

A. Cr_2O_3

The % Theoretical Density and the % Weight Loss of pure (99.99%) Cr_2O_3 and Cr_2O_3 with minor additions of MgO are plotted against the P_{O_2} in Figures 3, 6 and 7. The very strong dependence of density on P_{O_2} is shown in all three figures. The maximum density was obtained at the equilibrium P_{O_2} (2×10^{-12} atm) for the reaction

$$\frac{4}{3} Cr + O_2 = \frac{2}{3} Cr_2O_3 \qquad (8)$$

at 1600°C. The density decreased both at higher P_{O_2} where Cr_2O_3 is stable and at lower P_{O_2} where reduced Cr is stable. It dropped very markedly in the range $10^{-10} < P_{O_2} < 10^{-9}$ atm and continued to gradually decrease with increase in P_{O_2} through 1 atm.

Cr_2O_3 dissociates into several principal volatile species at 1600°C, in particular Cr, CrO, CrO_2, and CrO_3. The amount of volatilization of each species depends not only on the temperature, but also the P_{O_2} as shown by Grimley et. al.[15] The volatilization of these species has a significant effect on both the densification and the weight loss of Cr_2O_3. This work shows that controlling the P_{O_2} during the sintering of Cr_2O_3 will control the volatilization of various Cr-O species and in turn control the densification of the Cr_2O_3. The exact mechanism of increase in density with decrease in P_{O_2} was

not determined, but possible mechanisms will be discussed later in the discussion.

The experimental weight loss dependence of the pure Cr_2O_3 on the P_{O_2} is shown on Figure 3. The general form of this dependence can be explained by considering the vapor-pressure dependence of the most volatile species on P_{O_2}. Due to lack of data for some of these species some oversimplified assumptions will be made keeping in mind the limitations of the approach. Figure 4 is a Kellogg-type diagram for the Cr-O system at 1600°C drawn similar to the one by Graham and Davis[16] at 1200°C. This diagram assumes that CrO_3 is the only volatile oxide of chromium. This, of course, is not the case since CrO_2 and CrO must be considered. In fact, the mass spectrometry studies of Grimley et. al.[15] have pointed out that below $P_{O_2} \leq 10^{-7}$ atm CrO_3 is not detected at all and even at $P_{O_2} = 10^{-6}$ atm, the P_{CrO_2} is one hundred times the P_{CrO_3}. Neglecting the lower oxides such as CrO_2 as Graham et. al[16] have done is certainly not justified, but the same type of plot is used here to calculate the general trend of weight loss behavior expected, realizing that data on the lower oxides should refine the comparison with these experiments following Graham et. al.

The P_{Cr} was obtained from the equation[17]

$$\log P_{Cr} = \frac{-20,400}{T} + (-1.82) \log T + 16.23$$

P_{Cr} = partial pressure of Cr (mmHg)

T = temperature (°K)

Figure 3. The partial pressure of oxygen vs. density and weight loss of Cr_2O_3 at 1600°C for 1 hour

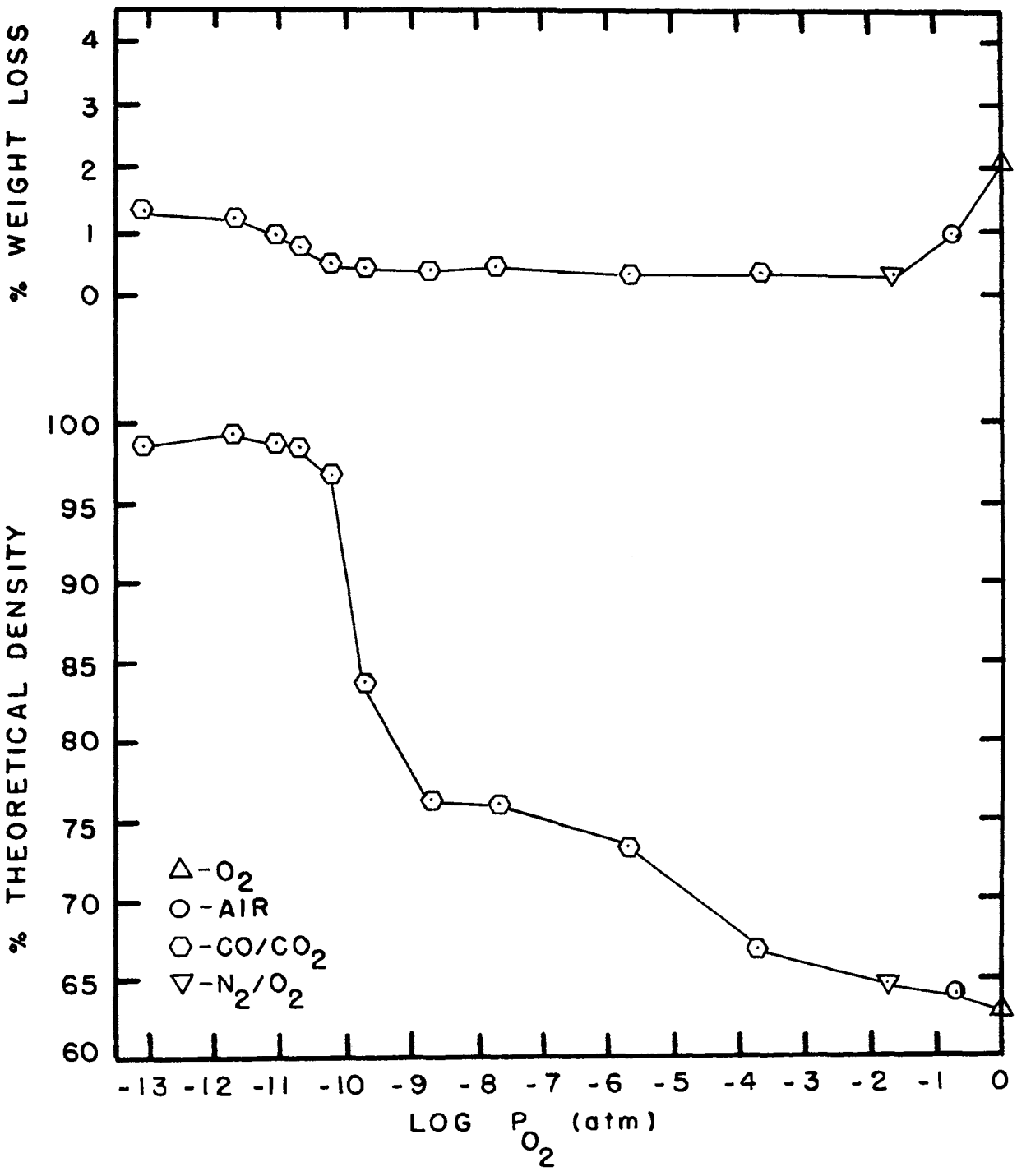
% WEIGHT LOSS
4
3
2
1
0
% THEORETICAL DENSITY
100
95
90
85
80
75
70
65
60
△-O2
○-AIR
⬡-CO/CO2
▽-N2/O2
-13 -12 -11 -10 -9 -8 -7 -6 -5 -4 -3 -2 -1 0
LOG PO2 (atm)

Figure 3

The P_{CrO_3} from the reaction

$$Cr_2O_3\ (s) + \frac{3}{2}\ O_2(g) = 2CrO_3(g)$$

was calculated from the equilibrium constant expression

$$K = \frac{(P_{CrO_3})^2}{(P_{O_2})^{3/2}}$$

by solving for P_{CrO_3}

$$P_{CrO_3} = K^{1/2}\ (P_{O_2})^{3/4}$$

and using the equilibrium constant expression[16] for this reaction, from the literature.

$$\log K = \frac{-2.46 \times 10^4}{T} + 6.16$$

The theoretical weight loss was then determined by substituting the P_{Cr}, and P_{CrO_3} obtained from Figure 4 at various partial pressures into the Langmuir evaporation equation[17]

$$P = 0.02256\ \frac{M}{t \cdot A}\ \sqrt{\frac{T}{M}} \qquad (9)$$

where P = partial pressure (atm)

m = mass of vapor (g)

t = time (sec)

A = surface area (cm^2)

T = temperature (°K)

M = molecular weight of gaseous species

(For calculations see Appendix B). This weight loss in relative units is plotted versus the P_{O_2} in Figure 5

Figure 4. Kellogg-type diagram for Cr-O system at 1600°C. (Neglecting all vapor species except Cr and CrO_3 following Graham et. al.[16])

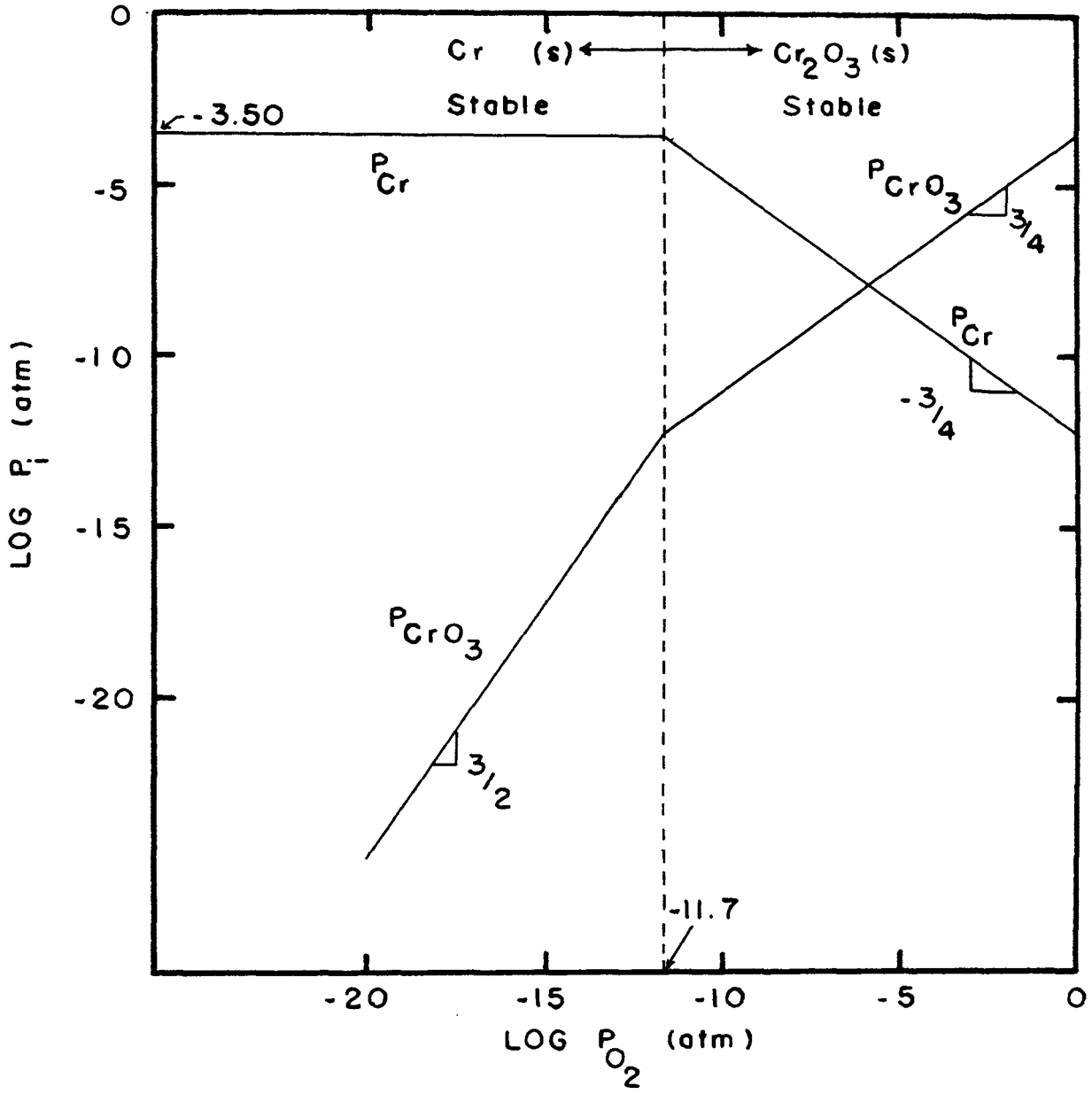
Cr (s) ⟷ Cr2O3 (s)
Stable
Stable
-3.50
PCr
PCrO3
3/4
PCr
-3/4
PCrO3
3/2
-11.7
0
-5
-10
-15
-20
LOG Pi (atm)
-20
-15
-10
-5
0
LOG PO2 (atm)

Figure 4

Figure 5. Calculated weight loss dependence on P_{O_2} in the Cr-O system at 1600°C. Based on calculations from vapor pressure data (a) solid curve from Figure 4 (b) dotted curve from Grimley et. al[6] and other vapor pressure data[17,18].

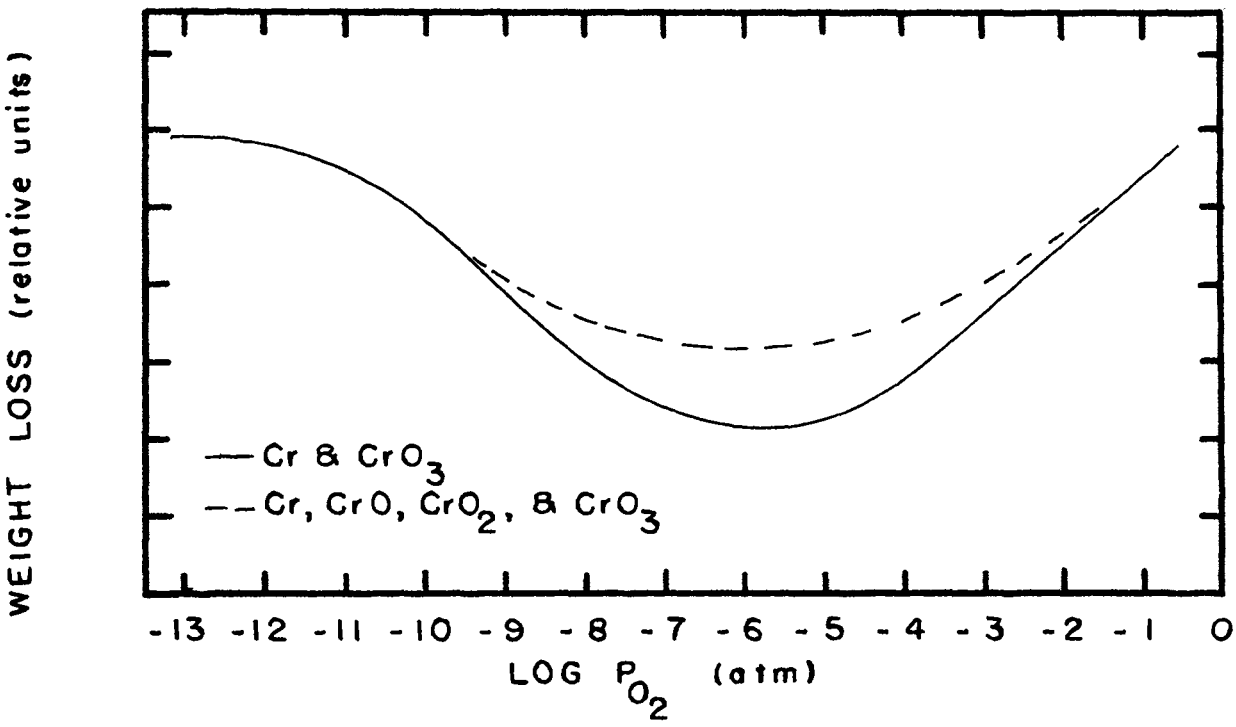
WEIGHT LOSS (relative units)
— Cr & CrO_3
-- Cr, CrO, CrO_2, & CrO_3
-13 -12 -11 -10 -9 -8 -7 -6 -5 -4 -3 -2 -1 0
LOG P_{O_2} (atm)

Figure 5

and compares generally with the experimental weight loss at $P_{O_2} \leq 2x10^{-12}$ in Figure 5 is consistent with the relatively constant % weight loss data for $P_{O_2} \leq 2x10^{-12}$ shown in Figure 3. This constant weight loss is a result of the constant vapor pressure of chromium metal as can be seen in Figure 4. Examination of the microstructure of polished samples fired in this P_{O_2} range revealed a shing second phase. X-ray diffraction and microprobe analysis failed to identify metallic chromium probably due to the minute quantity present.

In the P_{O_2} range of $2x10^{-12} < P_{O_2} < 2x10^{-6}$ atm the weight loss decreases (Figure 5) due to a decrease in the volatilization of Cr (Figure 4). From a $P_{O_2} = 2x10^{-6}$ to 1 atm the weight loss then increases due to increased volatilization of CrO_3. Figure 3 shows experimentally that the weight loss started to decrease with increase in P_{O_2} above $2x10^{-12}$ atm. However, at $P_{O_2} \simeq 2x10^{-10}$ to $2x10^{-2}$ the % weight loss remained relatively constant. This constant section of the curve is not seen theoretically when only the two vapor species i.e. Cr and CrO_3 are

considered as in Figure 5. If data were available however this central portion of the curve would be more nearly level. This trend was demonstrated by taking data from Grimley et. al. and adding in the expected loss due to CrO and CrO_2 (dashed curve Fig. 5) although this too must be considered rough since the needed data was meager. This again demonstrates the failure of considering just one oxide vapor species.

It can also be seen in Figures 4 and 5 as pointed out by Grimley et. al. that the presence of CrO_3 just starts to become significant at $P_{O_2} = 10^{-6}$ atm. CrO_3 does not add significantly to the weight loss data (Figure 3) until a $P_{O_2} > 2x10^{-2}$ atm. Hench[5] compared P_{CrO_3} obtained from firing his samples of Cr_2O_3 in air with the data of Parravano[18] and Alexander[5] who also performed some firings of Cr_2O_3 in air. He used the Langmuir evaporation equation to obtain the P_{CrO_3}. The work of these three investigators was performed in air at temperatures lower than 1600°C. Extrapolation of their work to 1600°C resulted in the following P_{CrO_3} for $P_{O_2} = 2x10^{-1}$ atm (air)

Hench	7.9×10^{-4} atm
Alexander	3.2×10^{-4} atm
Parravano	3.9×10^{-5} atm

The value of P_{CrO_3} indicated on the Kellogg-type diagram (Figure 4) is 10^{-4} atm while the value obtained by putting the weight loss in air data from these experiments in-

to the Langmuir expression is 10^{-5} atm (using the same assumptions as Hench[5]).

Having observed the oxygen pressure dependence of the density and weight loss one can now consider the possible mechanisms which aid sintering as the optimum density is approached. The decrease in P_{O_2} could create more oxygen vacancies. Since O^{2-} is the rate controlling species in the diffusion of Cr_2O_3 (O^{2-} diffusion coefficient is $\sim 10^4$ lower than that for Cr^{3+}), this could very well increase the densification of Cr_2O_3. In addition the P_{O_2} affects the amount and type of gaseous species present. The greater the volatilization the greater the number of pores which need to be eliminated by vacancy diffusion or by gaseous diffusion. The rate at which the gaseous species diffuse out of closed pores in the later stages of sintering will depend on the diffusivity of the gaseous species. It seems reasonably certain that near the optimum P_{O_2} for sintering, where high densities are achieved, the CrO_3 diffusivity is not important since it is not the primary vapor species in this P_{O_2} range.

B. MgO Additions to Cr_2O_3

The addition of MgO aided in the densification of the Cr_2O_3. The density data for 0.1 wt.% and 1.0 wt.% MgO as a function of P_{O_2} are shown on Figures 6 and 7 respectively. The addition of only 0.1 wt.% MgO enabled the Cr_2O_3 to sinter to nearly theoretical density (99.8%) in only 1 hour in a $P_{O_2} = 2x10^{-12}$ (the equilibrium P_{O_2} needed to maintain the Cr_2O_3 phase). The mechanism of sintering for Cr_2O_3 when not in a highly oxidizing atmosphere appears to be volume diffusion. When 2 Mg^{2+} ions substitute for 2 Cr^{3+} ions an oxygen vacancy is created thus enhancing the diffusion of the rate controlling species thereby aiding sintering. Another way that the MgO could aid in sintering Cr_2O_3 to nearly theoretical density is by solute segregation at the Cr_2O_3 grain boundaries. This may decrease the rate of grain growth and enable pores to be eliminated before being engulfed in the center of large grains where elimination is extremely slow due to the large diffusion path length.

The addition of 1.0 wt.% MgO (Figure 7), however, probably exceeded the solid solution limit of MgO in Cr_2O_3. The excess additive probably formed a spinel ($Mg\ Cr_2O_4$) with the Cr_2O_3 slowing the diffusion rate through these regions. The result was a decrease in density relative to the Cr_2O_3 with 0.1 wt.% MgO. This has been suggested to occur in the Al_2O_3-MgO system where MgO was the additive[2].

Figure 6. The partial pressure of oxygen vs. density and weight loss of Cr_2O_3 + 0.1 wt.% MgO at 1600°C for 1 hour.

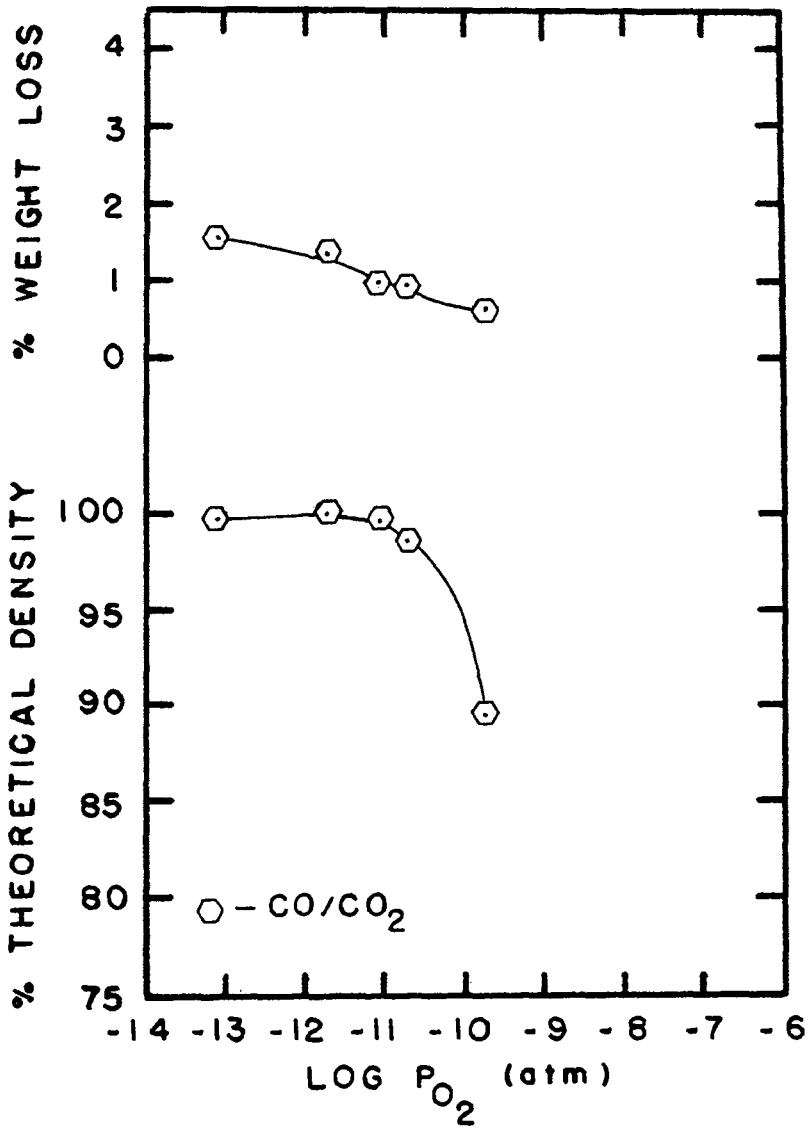
% WEIGHT LOSS
4
3
2
1
0
% THEORETICAL DENSITY
100
95
90
85
80
75
○ – CO/CO2
-14 -13 -12 -11 -10 -9 -8 -7 -6
LOG PO2 (atm)

Figure 6

Figure 7. The partial pressure of oxygen vs. density and weight loss of Cr_2O_3 + 1.0 wt.% MgO at 1600°C for 1 hour.

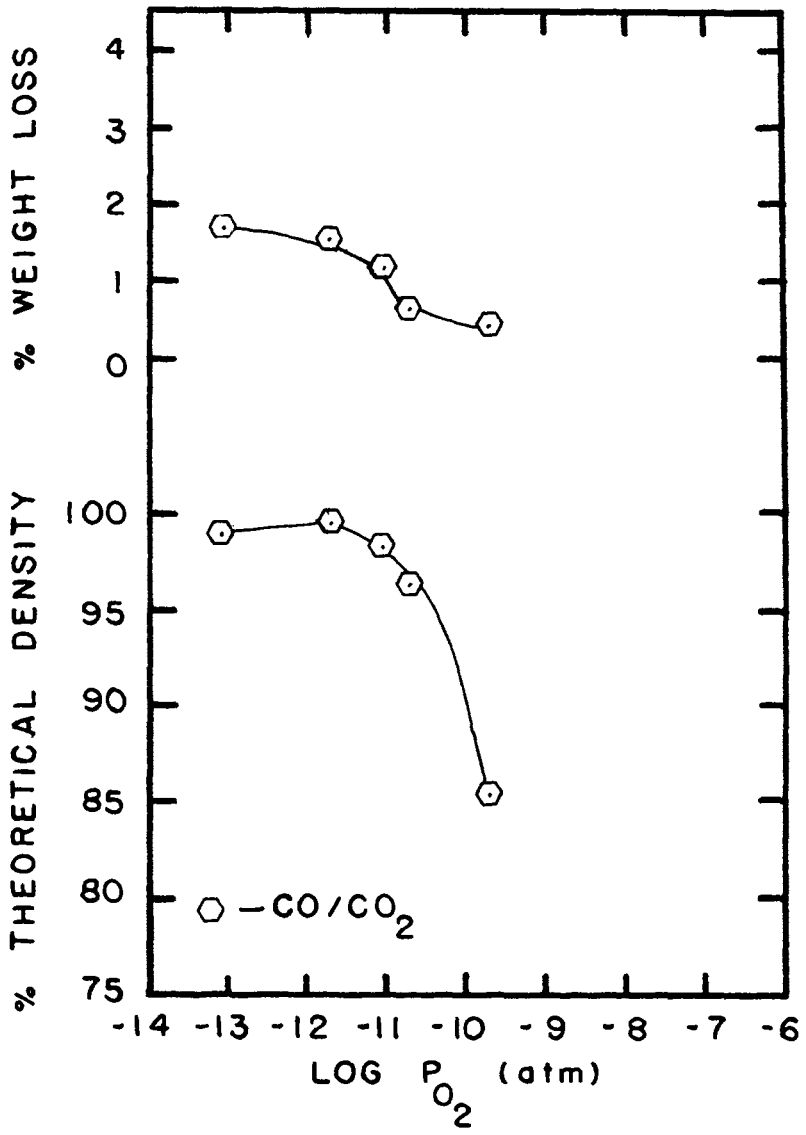
% WEIGHT LOSS
4
3
2
1
0
% THEORETICAL DENSITY
100
95
90
85
80
75
—CO/CO2
-14 -13 -12 -11 -10 -9 -8 -7 -6
LOG PO2 (atm)

Figure 7

Scanning electron micrographs of fractured surfaces from selected samples are shown on Figures 8, 9, 10, 11, and 12. Figure 8 is typical of the type of fine grain, highly porous, only partially sintered structure, which is produced when the partial pressure of oxygen is too high. Figure 9 represents the dense almost void free microstructure which results when the oxygen pressure is optimized. When the oxygen pressure gets too low, then intergranular pores again become plentiful (Figure 10). Figure 11 represents a specimen with 0.1 wt.% MgO added which was sintered in the optimum P_{O_2}. Note the very dense more uniform grain structure. A striking difference between the fractured surfaces of dense Cr_2O_3 with MgO additions and those without is apparent. The pure Cr_2O_3 sintered compacts break more frequently on the grain boundaries although many fractures across grains occur. The sample in Figure 10 with 0.1 wt. % MgO shows much more fracture through grains rather than at the boundaries. The grain boundaries seem to be "pinned" together more tightly. Considerable light is thrown on a mechanism for this grain boundary "pinning" mechanism by observing an occasional non-typical large grain which has fractured along a boundary. Figure 12 shows such a case where particles or nuclei of MgO or Mg-Cr spinel have segregated at the boundary effectively acting as pins which resist fracture along grain boundaries. Some of the pore like structures are no doubt craters left by those nuclei or particles

Figure 8. Scanning electron micrographs of Cr_2O_3 fired for 1 hour at 1600°C in a partial pressure of oxygen of $2x10^{-10}$ atm.

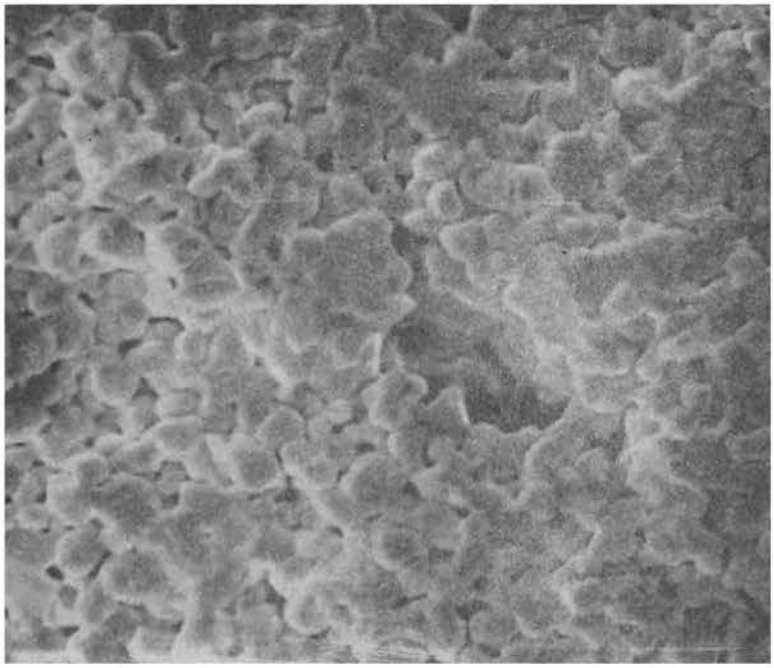

(a) 1000x

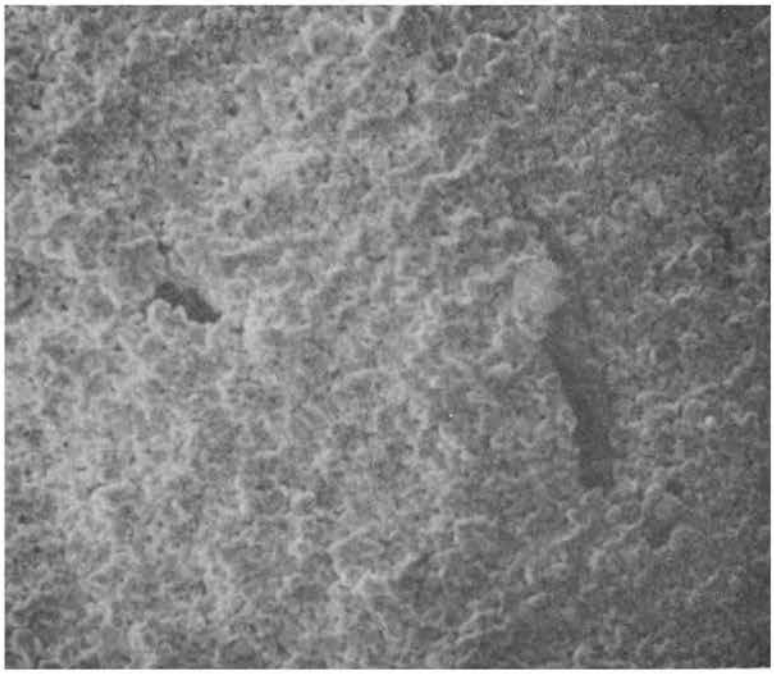

(b) 500x

Figure 8

Figure 9. Scanning electron micrographs of Cr_2O_3 fired for 1 hour at 1600°C in a partial pressure of oxygen of $2x10^{-12}$ atm.

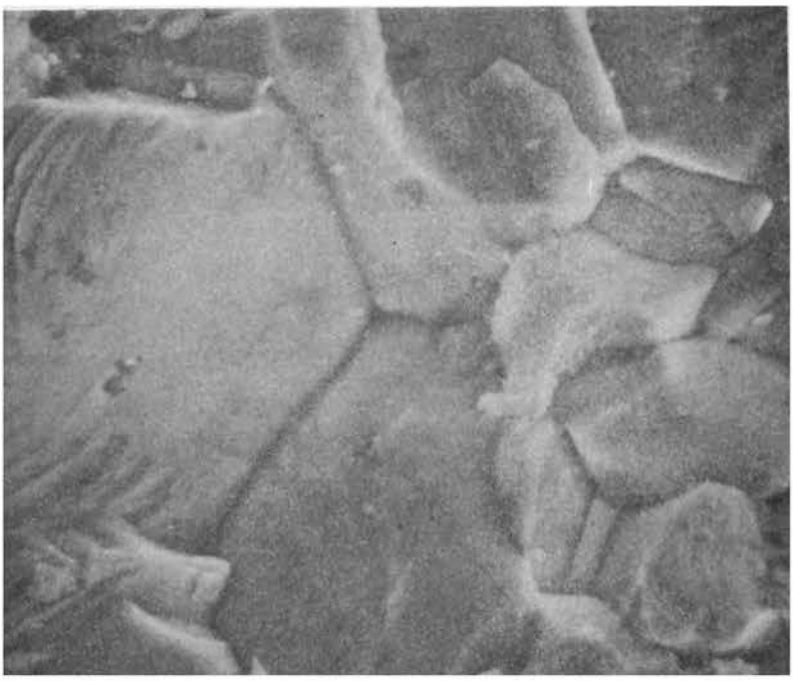

(a) 1000x

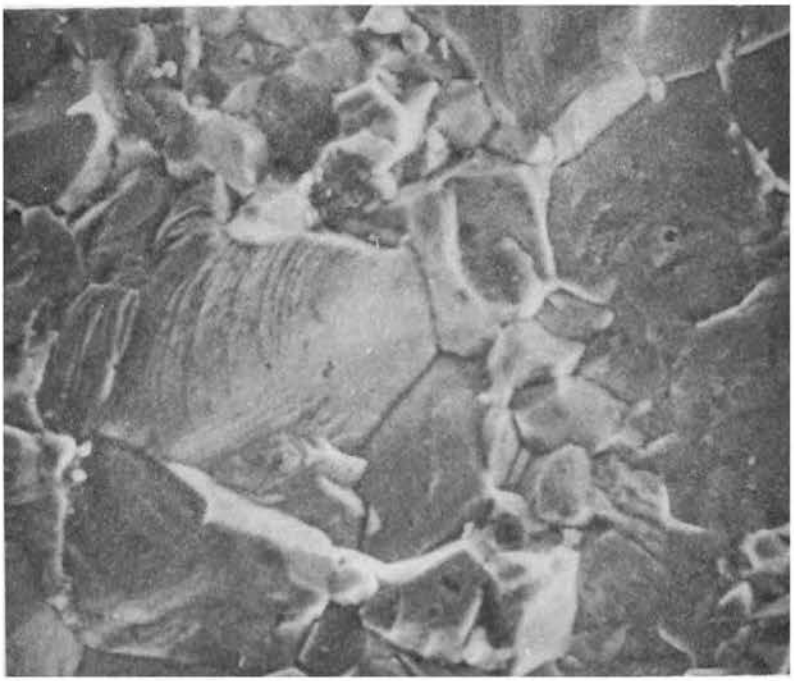

(b) 500x

Figure 9

Figure 10. Scanning electron micrograph of Cr_2O_3 fired for 1 hour at 1600°C in a partial pressure of oxygen of $9x10^{-14}$.

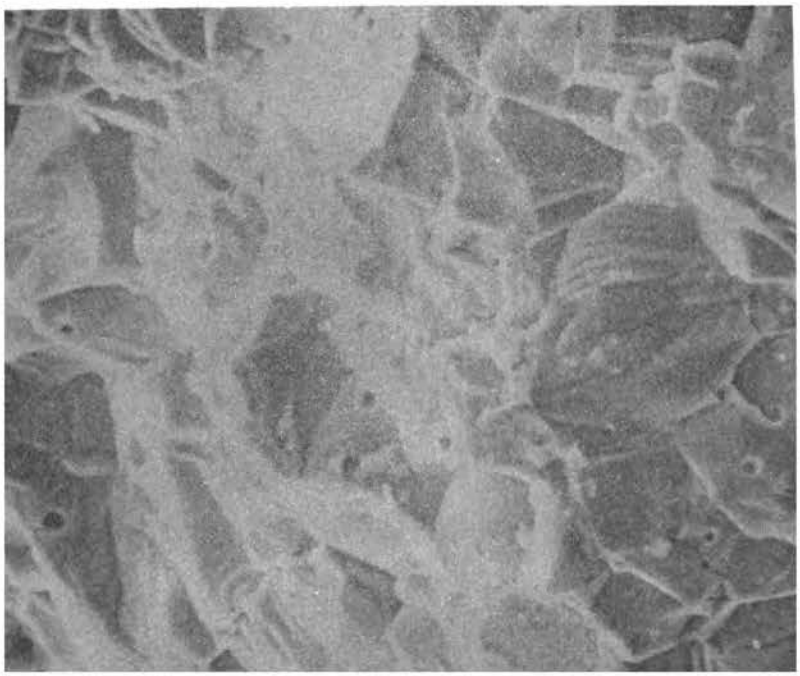

(500x)

Figure 10

Figure 11. Scanning electron micrographs of Cr_2O_3 + 0.1 wt. % MgO fired for 1 hour at 1600°C in a partial pressure of oxygen of $2x10^{-12}$ atm.

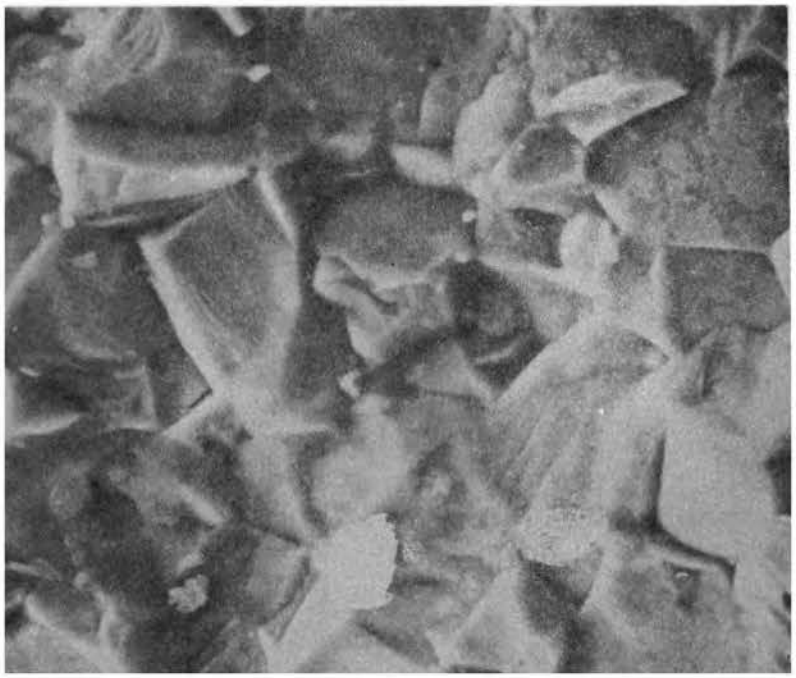

(a) 1000x

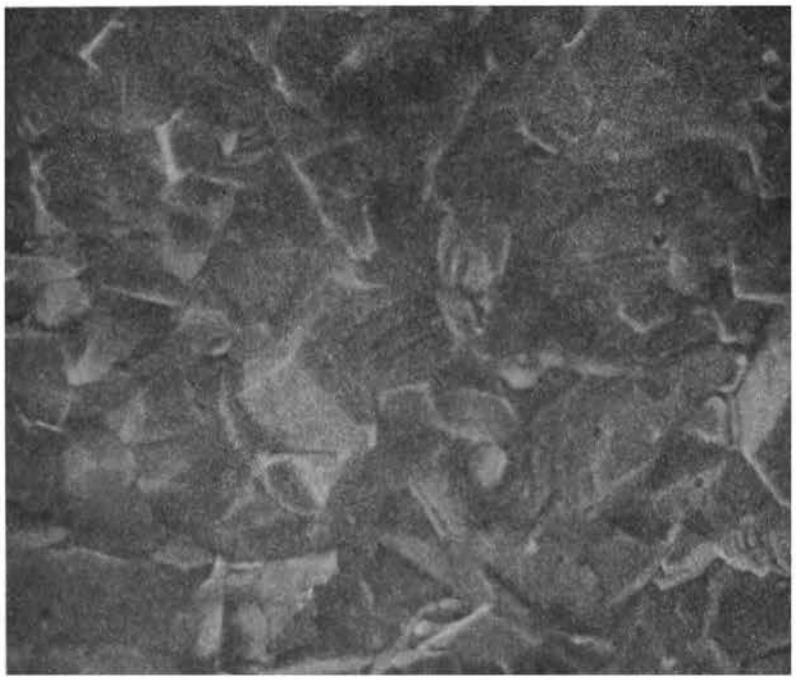

(b) 500x

Figure 11

Figure 12. Scanning electron micrograph of Cr_2O_3 + 0.1 wt.% MgO fired for 1 hour at 1600°C in a partial pressure of oxygen of $2x10^{-12}$ atm.

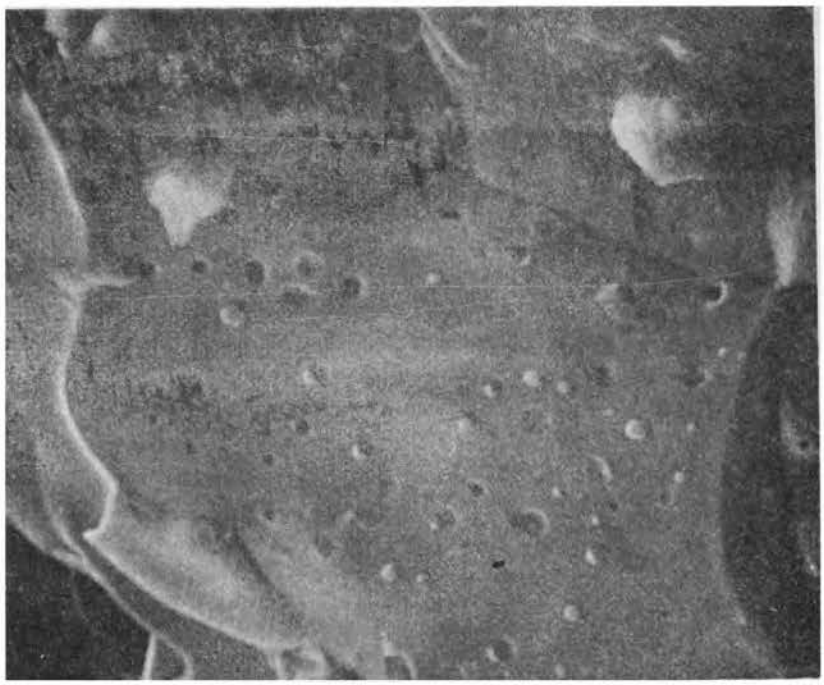

(500x)

Figure 12

which were pulled out during fracture and remain with the mating surface. Such particles also account for the smaller more uniform grain size of the 0.1% MgO specimens.

The CO/CO_2 buffer system was much easier to control than the H_2/H_2O buffer system. Figure 13 shows a few points obtained using the H_2/H_2O system. The density of the Cr_2O_3 did not drop as sharply at $P_{O_2} = 10^{-10}$ as in the CO/CO_2 system. This may indicate that the H_2 was not saturated with as much water vapor as assumed. Also observed from Figure 13 was the higher % weight loss.

C. Magnesium Oxide

The P_{O_2} region that the Cr_2O_3 samples were fired in was far above the equilibrium P_{O_2} for the reaction $2Mg + O_2 = 2MgO$ (approximately 10^{-20} atm), and therefore MgO is expected to be stable with respect to P_{O_2} in this P_{O_2} range. Since Mg^{++} does not tend to change oxidation state producing more volatile oxides, the effect of P_{O_2} on the sintering of MgO was expected to be little if any. Figure 14 is a plot of % Weight Loss and % Theoretical Density of MgO against the P_{O_2} investigated. The greatest color changes occurred in the P_{O_2} regions that corresponded to the areas of greatest weight loss in the Cr-O system, Figure 1, $9x10^{-14}$ and 0.2 atm. The MgO sample fired in a $P_{O_2} = 0.2$ atm was discolored a light green. This indicated that residual

Figure 13. The partial pressure of oxygen vs. density and weight loss of Cr_2O_3 at 1600°C for 1 hour using the H_2/H_2O buffer system.

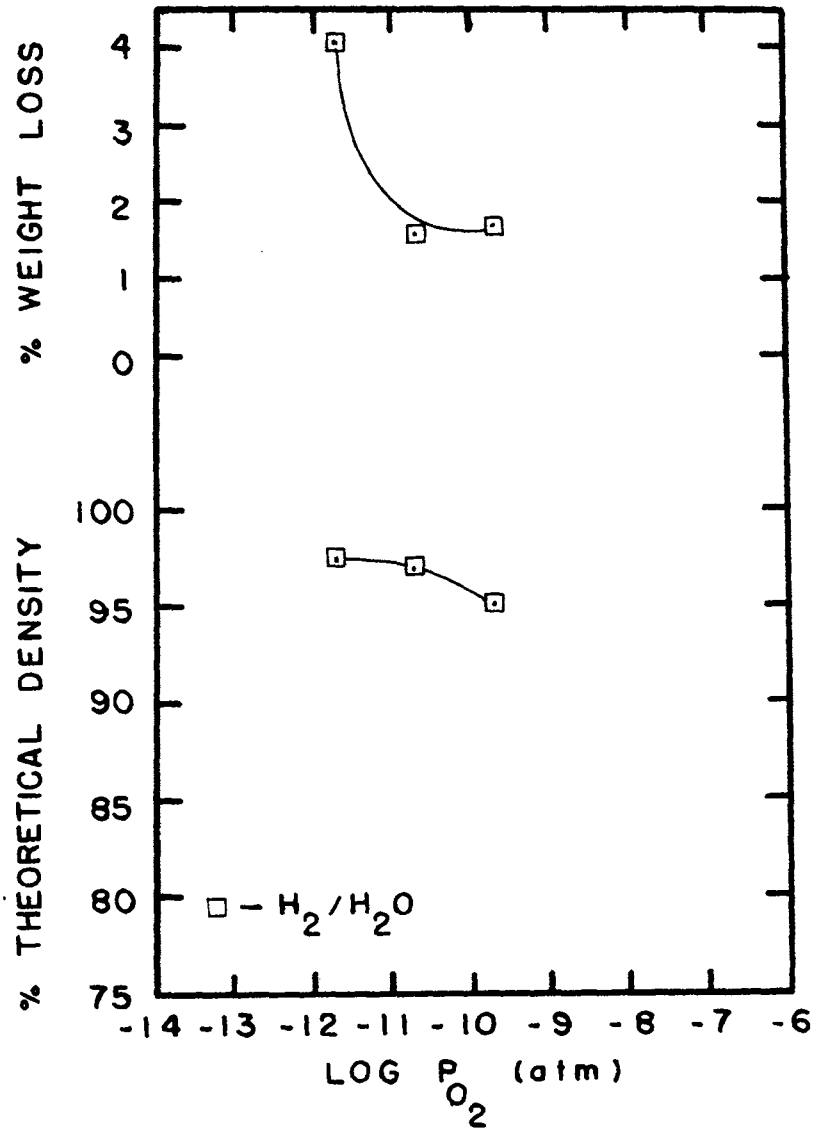
% WEIGHT LOSS
4
3
2
1
0
% THEORETICAL DENSITY
100
95
90
85
80
75
□ – H_2/H_2O
-14 -13 -12 -11 -10 -9 -8 -7 -6
LOG P_{O_2} (atm)

Figure 13

Figure 14. The partial pressure of oxygen vs. density and weight loss of MgO at 1600°C for 1 hour.

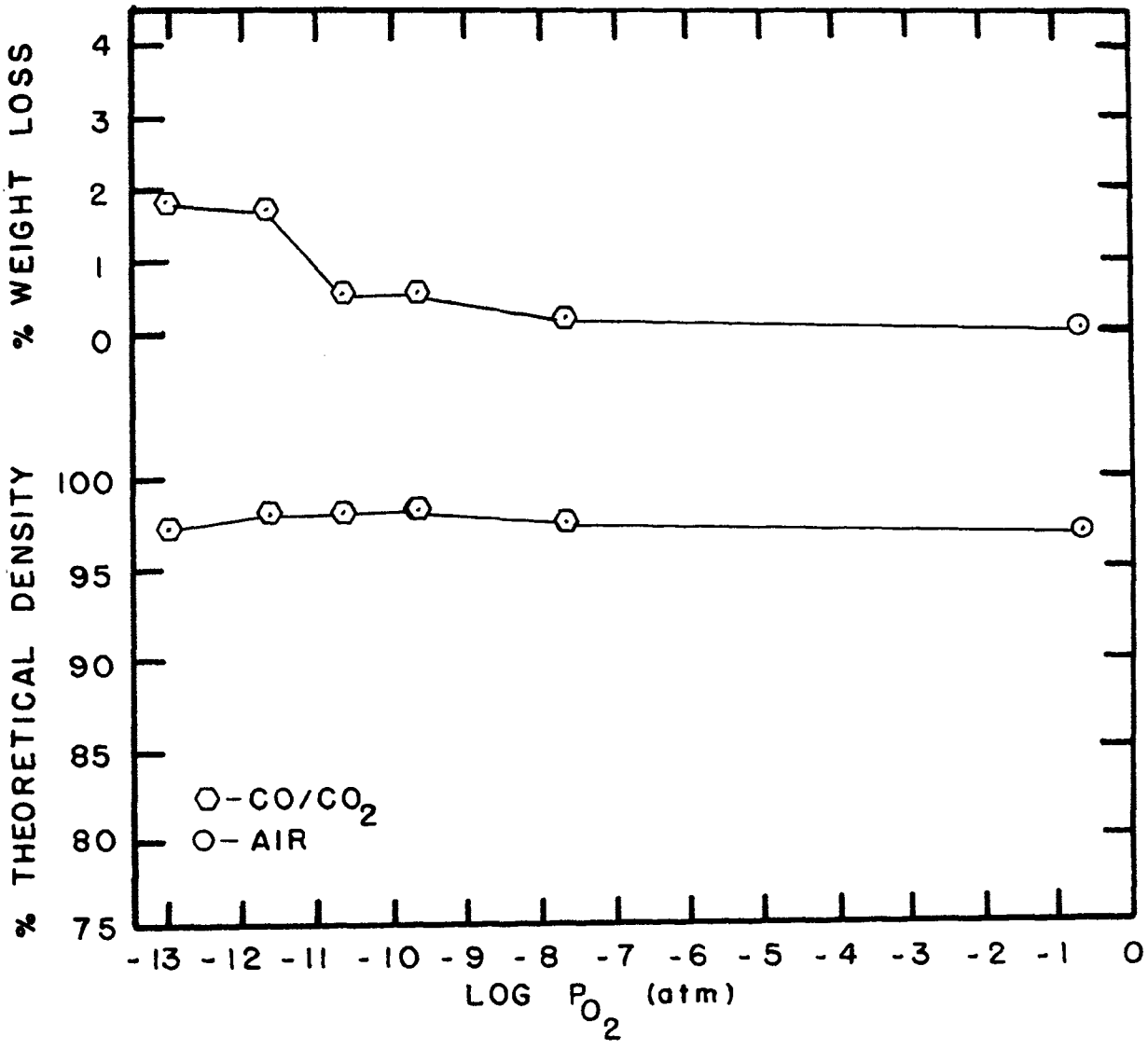
% WEIGHT LOSS
4
3
2
1
0
% THEORETICAL DENSITY
100
95
90
85
80
75
⬡-CO/CO2
○-AIR
-13 -12 -11 -10 -9 -8 -7 -6 -5 -4 -3 -2 -1 0
LOG PO2 (atm)

Figure 14

vapors present in the furnace from previous Cr_2O_3 firings affected the sintering of the MgO. The most predominant gaseous species of the Cr-O system in the P_{O_2} = 0.2 atm is CrO_3. Since CrO_3 has been shown to be detrimental to the sintering of MgO[5], the slightly lower density at this P_{O_2} is understandable. The MgO samples fired at $9x10^{-14}$ and $2x10^{-12}$ were discolored a tannish green and a light green respectively. The samples fired in $P_{O_2} > 2x10^{-12}$ but < 0.2 atm were pure white. The predominant gaseous species of the Cr-O system present in the $P_{O_2} = 9x10^{-14}$ through 10^{-10} is Cr. The decrease in discoloration with increase in P_{O_2} follows since the P_{Cr} decreases with increase in P_{O_2}. A slight increase in the density and a relatively large decrease in weight loss was also noted with the increase in P_{O_2}. Thus, the Cr vapor was not only detrimental to the MgO in densification, but it also caused greater than expected weight loss. Unlike the Cr vapor, the CrO_3 did not increase the weight loss of the MgO. The mechanism of the phenomenon is still not understood and would be interesting for future studies.

The addition of Cr_2O_3 to MgO did not change the general trend of the density and weight loss of MgO, Figures 15, 16, and 17, with increase in P_{O_2}. The density of the MgO increased gradually through the P_{O_2} region $2x10^{-12}$ to $2x10^{-10}$. The increase became somewhat sharper with increase in Cr_2O_3 additions. The density also decreased with higher Cr_2O_3 additions at each P_{O_2}. The

Figure 15. The partial pressure of oxygen vs. density and weight loss for MgO + 0.8 wt.% Cr_2O_3 at 1600°C for 1 hour.

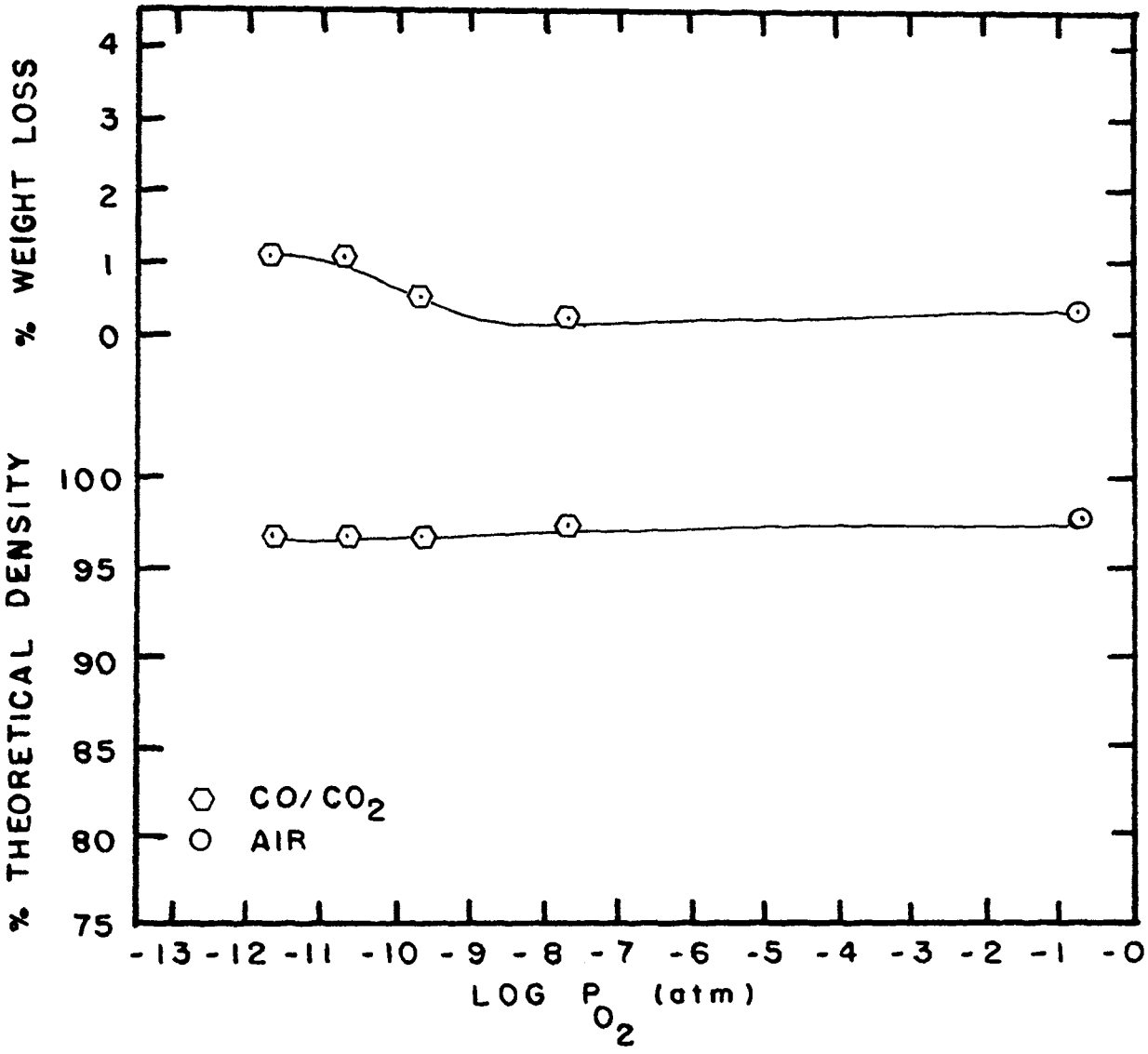
% WEIGHT LOSS
4
3
2
1
0
% THEORETICAL DENSITY
100
95
90
85
80
75
CO/CO2
AIR
-13 -12 -11 -10 -9 -8 -7 -6 -5 -4 -3 -2 -1 -0
LOG P O2 (atm)

Figure 15

Figure 16. The partial pressure of oxygen vs. density and weight loss of MgO + 2.0 wt.% Cr_2O_3 at 1600°C for 1 hour.

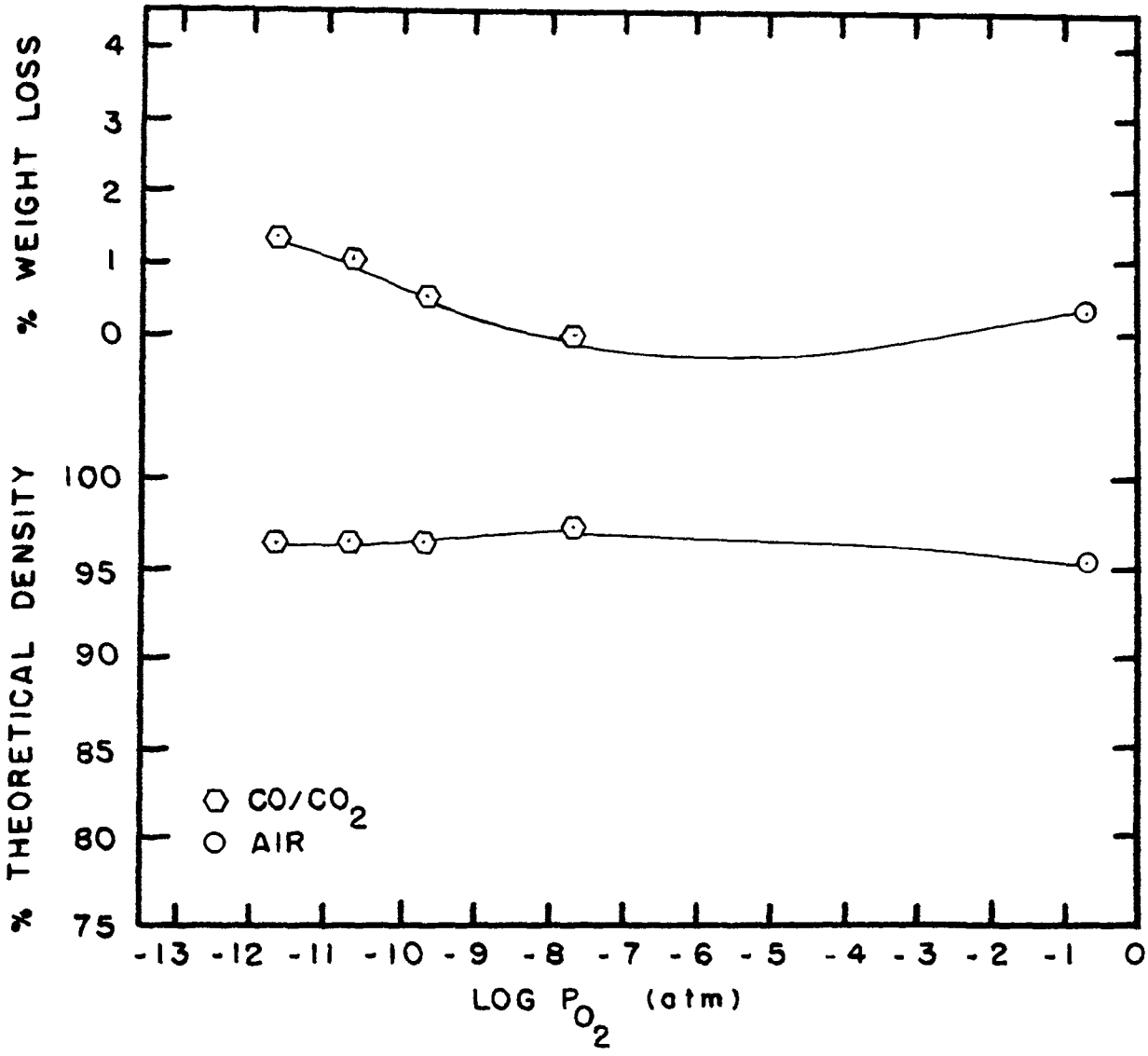
% WEIGHT LOSS
4
3
2
1
0
% THEORETICAL DENSITY
100
95
90
85
80
75
CO/CO2
AIR
-13 -12 -11 -10 -9 -8 -7 -6 -5 -4 -3 -2 -1 0
LOG PO2 (atm)

Figure 16

Figure 17. The partial pressure of oxygen vs. density and weight loss of MgO + 4.0 wt.% Cr_2O_3 at 1600°C for 1 hour.

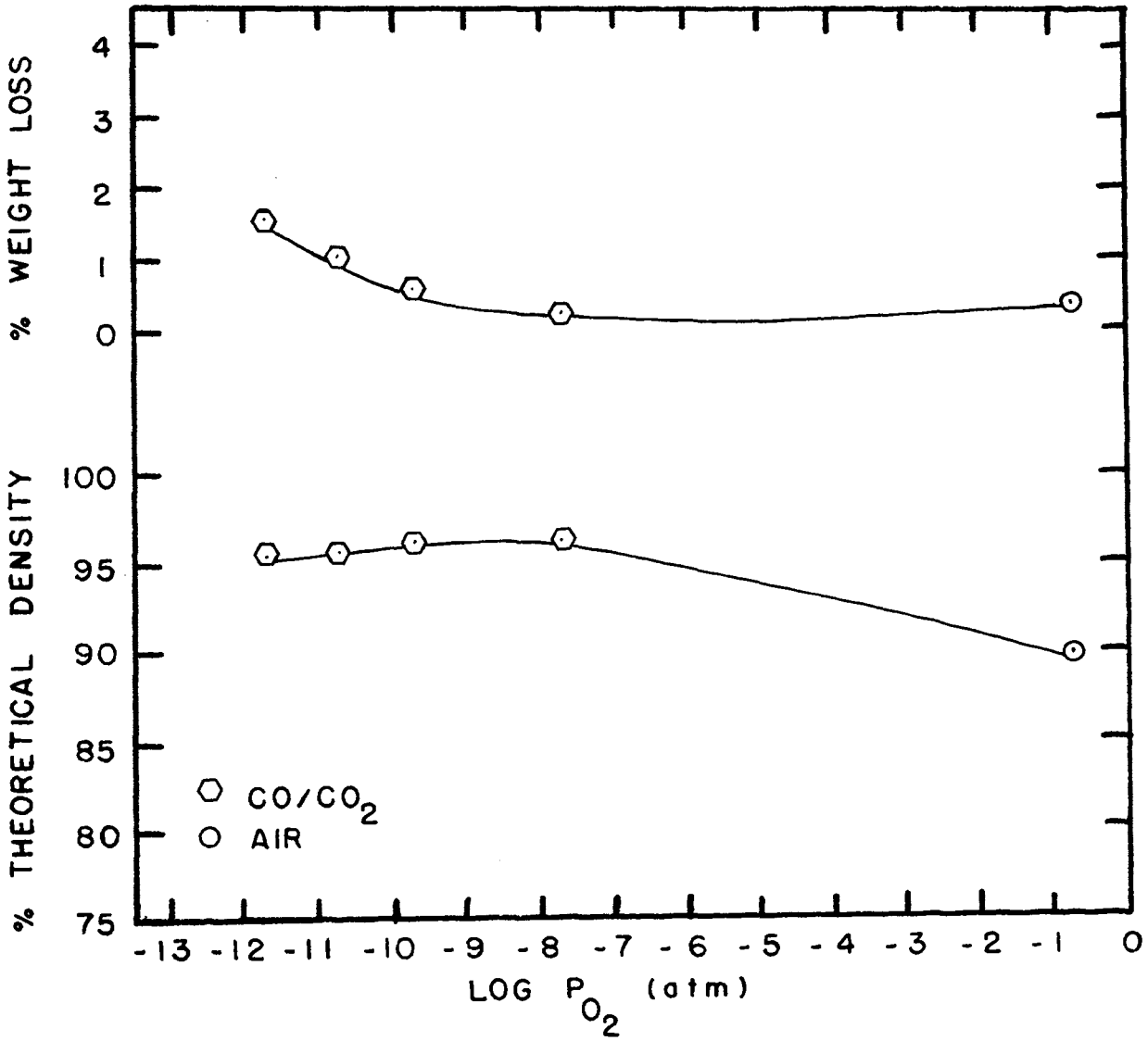
% WEIGHT LOSS
4
3
2
1
0
% THEORETICAL DENSITY
100
95
90
85
80
75
CO/CO2
AIR
-13 -12 -11 -10 -9 -8 -7 -6 -5 -4 -3 -2 -1 0
LOG PO2 (atm)

Figure 17

density decreased the most in a P_{O_2} = 0.2 atm. The weight loss was increased significantly compared to the MgO without the additive in this same P_{O_2}. This was probably due to volatilization of the CrO_3 from the Cr_2O_3 in the MgO sample.

Figure 18, shows the density and weight loss of MgO as a function of oxygen partial pressure in a H_2/H_2O buffer system. The weight loss was increased relative to the samples fired in the CO/CO_2 buffer system. Increased weight loss was also noted on the Cr_2O_3 side of the Cr_2O_3-MgO binary in the same buffer system.

It was thought at first that water vapor in the H_2/H_2O buffer system could be affecting the sintering of the MgO. It has been shown by Anderson and Morgan[19] that water vapor increases the rate of crystal growth of MgO. Rapid crystal growth can be detrimental to sintering. Figure 19 shows MgO sintered in a N_2 atmosphere with increased quantities of H_2O vapor. The only significant effect was an increase in density relative to firing in just N_2.

Figure 18. The partial pressure of oxygen vs. density and weight loss of MgO at 1600°C for 1 hour using the H_2/H_2O buffer system.

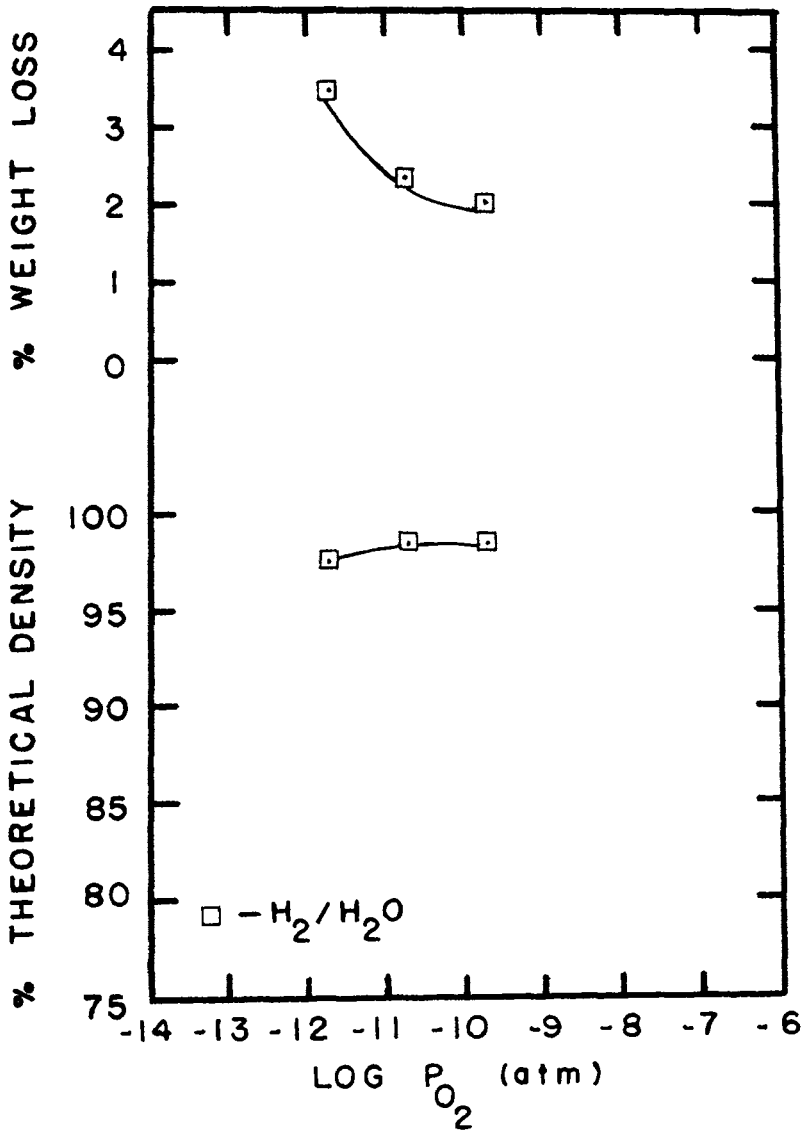
% WEIGHT LOSS
4
3
2
1
0
% THEORETICAL DENSITY
100
95
90
85
80
75
□ – H_2/H_2O
-14 -13 -12 -11 -10 -9 -8 -7 -6
LOG P_{O_2} (atm)

Figure 18

Figure 19. The partial pressure of oxygen vs. density and weight loss of MgO at 1600°C for 1 hour using the N_2/H_2O system.

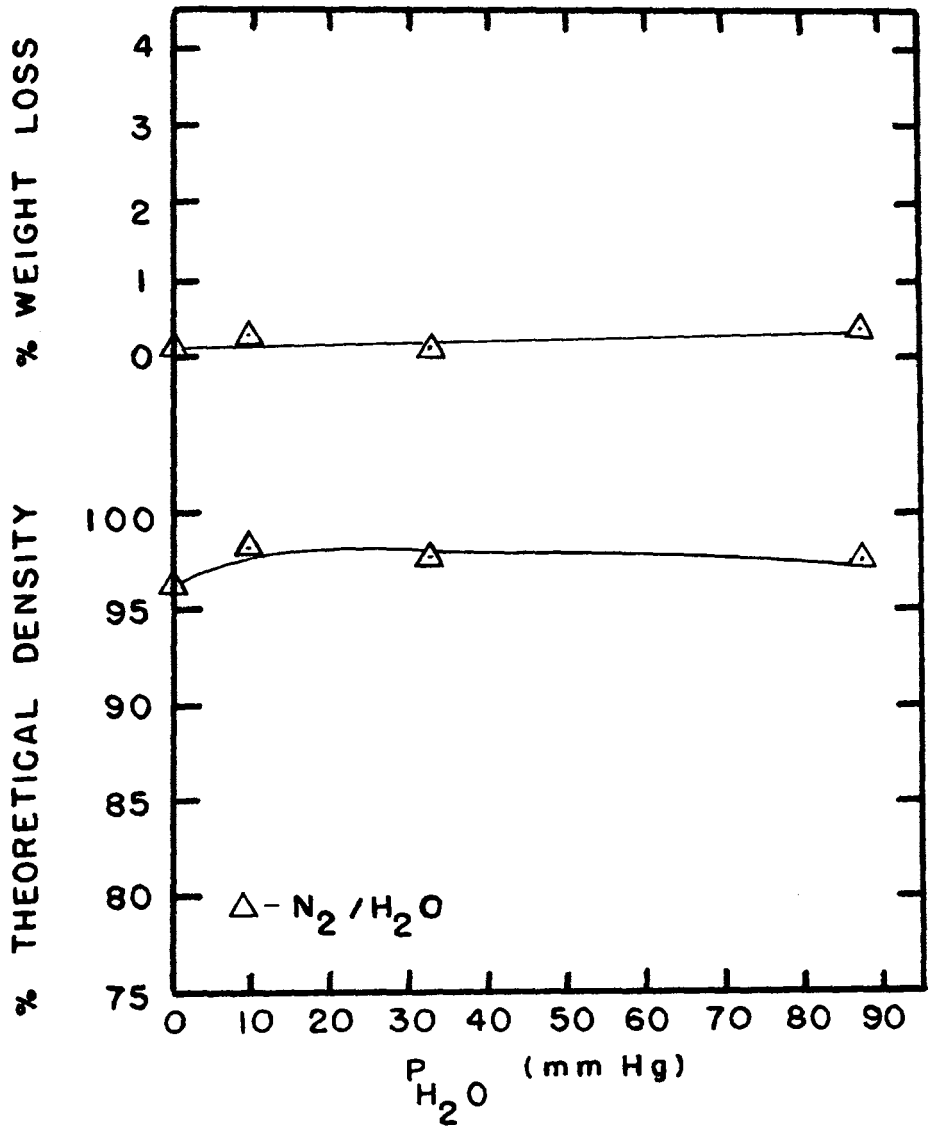
% WEIGHT LOSS
4
3
2
1
0
% THEORETICAL DENSITY
100
95
90
85
80
75
△- N_2 / H_2O
0 10 20 30 40 50 60 70 80 90
P_{H_2O} (mm Hg)

Figure 19

TABLE III

Data on Cr_2O_3 Samples Fired in CO/CO_2 Buffer System

Wt.% MgO Addition	P_{O_2} (atm)	Surface Area	Weight Loss	% Weight Loss	Green Density	Fired Density	% Theoretical Density
0	$9x10^{-14}$	$4.303cm^2$	0.0251g	1.34	3.290g/cc	5.14 g/cc	98.6
0	$2x10^{-12}$	4.320	0.0229	1.23	3.254	5.18	99.4
0	$9x10^{-12}$	4.484	0.0197	0.96	3.262	5.15	98.8
0	$2x10^{-11}$	4.524	0.0161	0.78	3.251	5.10	98.6
0	$6x10^{-11}$	4.353	0.0102	0.53	3.282	5.04	96.8
0	$2x10^{-10}$	-	0.0103	0.49	-	4.36	83.7
0	$2x10^{-9}$	4.484	0.0086	0.42	3.275	3.97	76.2
0	$2x10^{-8}$	4.504	0.0096	0.47	3.221	3.96	76.0
0	$2x10^{-6}$	4.164	0.0050	0.31	3.172	3.81	73.2
0	$2x10^{-4}$	4.956	0.0085	0.33	3.305	3.47	66.6
0	$*2x10^{-2}$	4.841	0.0076	0.31	3.265	3.38	64.7
0	$**2x10^{-1}$	4.152	0.0164	0.96	3.288	3.33	64.0
0	***1	3.457	0.0268	2.02	3.291	3.28	62.9
0.1	$9x10^{-14}$	4.494	0.0325	1.54	3.349	5.19	99.6
0.1	$2x10^{-12}$	4.721	0.0319	1.34	3.367	5.20	99.8

* N_2/O_2 *** O_2

** Air

TABLE III (Cont.)

Wt.% MgO Addition	P_{O_2} (atm)	Surface Area	Weight Loss	% Weight Loss	Green Density	Fired Density	% Theoretical Density
0.1	$9x10^{-12}$	4.323	0.0202	0.98	3.308	5.18	99.5
0.1	$2x10^{-11}$	4.666	0.0211	0.93	3.338	5.13	98.5
0.1	$2x10^{-10}$	4.239	0.0317	0.63	3.365	4.66	89.4
1.0	$9x10^{-14}$	4.651	0.0383	1.71	3.281	5.16	99.0
1.0	$2x10^{-12}$	4.065	0.0263	1.58	3.32	5.18	99.5
1.0	$9x10^{-12}$	3.982	0.0188	1.20	3.291	5.13	98.4
1.0	$2x10^{-11}$	4.099	0.0115	0.68	3.289	5.03	96.5
1.0	$2x10^{-10}$	4.115	0.0082	0.48	3.324	4.46	85.6

TABLE IV

Data on MgO Samples Fired in CO/CO_2 Buffer System

Wt.% Cr_2O_3 Addition	P_{O_2} (atm)	Surface Area	Weight Loss	% Weight Loss	Green Density	Fired Density	% Theoretical Density
0	$9x10^{-14}$	$4.085cm^2$	0.0167g	1.85	1.741g/cc	3.48 g/cc	97.2
0	$2x10^{-12}$	3.745	0.0133	1.74	1.805	3.51	97.9
0	$2x10^{-11}$	4.304	0.0061	0.57	1.793	3.51	98.0
0	$2x10^{-10}$	4.164	0.0060	0.59	1.818	3.51	98.1
0	$2x10^{-8}$	3.950	0.0021	0.23	1.821	3.49	97.4
0	*$2x10^{-1}$	3.950	0.0003	0.03	1.831	3.47	97.0
0.8	$2x10^{-12}$	6.992	0.0170	1.09	1.717	3.47	96.9
0.8	$2x10^{-11}$	7.134	0.0183	1.08	1.744	3.47	96.8
0.8	$2x10^{-10}$	6.995	0.0082	0.52	1.734	3.46	96.8
0.8	$2x10^{-8}$	7.037	0,0049	0.23	1.759	3.48	97.4
0.8	*$2x10^{-1}$	-	0.0025	0.34	-	3.49	97.6
2.0	$2x10^{-12}$	4.134	0.0130	1.37	1.762	3.45	96.4
2.0	$2x10^{-11}$	3.950	0.0093	1.03	1.861	3.46	96.5
2.0	$2x10^{-10}$	3.780	0.0044	0.54	1.900	3.46	96.5

* Air

TABLE IV (Cont.)

Wt.% Cr_2O_3 Addition	P_{O_2} (atm)	Surface Area	Weight Loss	% Weight Loss	Green Density	Fired Density	% Theoretical Density
2.0	$2x10^{-8}$	4.264	0.0000	0.00	1.878	3.48	97.3
2.0	*$2x10^{-1}$	4.012	0.0030	0.32	1.842	3.42	95.4
4.0	$2x10^{-12}$	4.019	0.0150	1.59	1.878	3.43	95.5
4.0	$2x10^{-11}$	4.108	0.0105	1.08	1.839	3.43	95.8
4.0	$2x10^{-10}$	4.006	0.0059	0.62	1.916	3.45	96.3
4.0	$2x10^{-8}$	4.048	0.0026	0.27	1.898	3.45	96.3
4.0	*$2x10^{-1}$	4.117	0.0035	0.34	1.907	3.22	89.9

* Air

TABLE V

Data on Samples Fired in Atmospheres With Water Vapor

H_2/H_2O

Sample Composition	P_{H_2O} (mmHg)	Surface Area	Weight Loss	% Weight Loss	Green Density	Fired Density	% Theoretical Density
MgO	9.8	3.901cm^2	0.0305g	3.48	1.858g/cc	3.49 g/cc	97.4
MgO	32.4	3.976	0.0205	2.37	1.764	3.52	98.4
MgO	87.7	3.872	0.0162	2.03	1.727	3.52	98.5
Cr_2O_3	9.8	3.911	0.0596	4.06	3.286	5.08	97.5
Cr_2O_3	32.4	5.012	0.0407	1.57	3.268	5.05	96.9
Cr_2O_3	87.7	5.082	0.0458	1.69	3.309	4.95	95.0
				N_2/H_2O			
MgO	0	3.963	0.0010	0.12	1.745	3.44	96.2
MgO	9.8	3.937	0.0024	0.27	1.829	3.51	98.2
MgO	32.4	3.963	0.0009	0.13	1.777	3.50	97.7
MgO	87.7	3.999	0.0028	0.33	1.727	3.49	97.4

V. CONCLUSIONS

The P_{O_2} greatly affects the sintering of Cr_2O_3. The maximum density obtained from sintering for 1 hour at 1600°C occurs in a $P_{O_2} = 2x10^{-12}$ atm which is the equilibrium P_{O_2} for the reaction $\frac{4}{3}$ Cr + O_2 = $\frac{2}{3}$ Cr_2O_3. P_{O_2} less and greater than $2x10^{-12}$ atm causes the density to decrease. The greatest decrease occurs at 10^{-10} atm where the other oxides of chromium begin to show significant volatilization and the Cr vapor begins to become insignificant.

In the partial pressure of oxygen range 10^{-10} to 10^{-2}, gaseous CrO and CrO_2 are present in significant quantities that cannot be ignored during the sintering process of Cr_2O_3.

The addition of only 0.1 wt.% MgO increases the sintered density of Cr_2O_3 in a $P_{O_2} = 2x10^{-12}$ atm to very nearly theoretical density in 1 hour at 1600°C. The mechanism seems to be due to pinning of the grain boundaries by particles or nuclei of MgO or Mg-Cr spinel that have segregated at the boundary. The addition of 1.0 wt.% MgO causes the sintered density to decrease relative to the density obtained with only 0.1 wt. % MgO. It was, however, denser than pure Cr_2O_3.

Sintering of Cr_2O_3 in a H_2/H_2O buffer system caused greater volatilization of the various gaseous species in the Cr-O system than in a CO/CO_2 buffer system. Therefore,

water vapor appears to be playing an important role in addition to just establishing the P_{O_2}. This data is inconclusive however, since this buffer system was harder to control and therefore abandoned.

The addition of Cr_2O_3 to MgO caused the density to decrease with increase in addition of Cr_2O_3 at 1600°C. The greatest decrease was noted in P_{O_2} where the Cr and CrO_3 vapor were the dominant gaseous species. Cr vapor also caused greater weight loss of MgO.

The presence of a small amount of water vapor slightly increased the sintered density of MgO compared to firing in dry N_2, but the sintered density remained constant with an increase in water vapor pressure.

BIBLIOGRAPHY

1. P. J. Jorgensen, "Modification of Sintering Kinetics by Solute Segregation in Al_2O_3," J. Am. Ceram. Soc., 48 (4), 207-10 (1965).

2. J. W. Nelson and I. B. Cutler, "Effect of Oxide Additions on Sintering of Magnesia," ibid, 41 (10), 406-9 (1958).

3. L. L. Hench and R. Russell, Jr., "Effect of Cr_2O_3 Vaporization on the Sintering of MgO," Trans. Brit. Ceram. Soc., 67 (9), 377-89 (1968).

4. G. K. Layden and M. C. McQuarrie, "Effect of Minor Additions on Sintering of MgO" J. Am. Ceram. Soc. 42 (2) 89-92 (1959).

5. L. L.Hench, "Sintering and Reactions of MgO and Cr_2O_3," Ph.D. dissertation, Ohio State Univ. (1964).

6. D. Caplan and M. Cohen, "The Volatilization of Chromium Oxide," J. Electrochem. Soc., 108, 438-42 (1961).

7. W. C. Hagel and A. V. Seybolt, "Cation Diffusion in Cr_2O_3", ibid. 108 (12) 1146-1152 (1961).

8. W. C. Hagel, "Anion Diffusion in α-Cr_2O_3," J. Am. Cer. Soc., 48 (2), 70-75 (1965).

9. W. C. Hagel, P. J. Jorgensen, and D. S. Tomalin, "Initial Sintering of α-Cr_2O_3," ibid, 49 (1), 23-26 (1966).

10. R. L. Coble, "Sintering Alumina: Effect of Atmospheres," ibid, 45 (3) 123-127 (1962).

11. J. T. Jones, P. K. Maitra and J. B. Cutler, "Role of Structural Defects in the Sintering of Alumina and Magnesia," ibid, 41 (9) 353-57 (1958).

12. P. J. Jorgensen and R. C. Anderson, "Grain-Boundary Segregation and Final-Stage Sintering of Y_2O_3," ibid, 50 (11), 553-8 (1967).

13. Richard A. Swalin, Thermodynamics of Solids, John Wiley & Sons, Inc. New York (1962).

14. L. S. Darken and R. W. Gurry, "The System Iron-Oxygen. I The Wüstite Field and Related Equilibria," J. Am. Chem. Soc. 67 1398 (1945).

15. R. T. Grimley, R. P. Burns, and M. G. Inghram, "Thermodynamics of the Vaporization of Cr_2O_3: Dissociation Energies of CrO, CrO_2, and CrO_3," J. of Chem. Physics, 34 (2) 664-671 (1961).

16. H. C. Graham and H. H. Davis, "Oxidation/Vaporization Kinetics of Cr_2O_3," J. Am. Ceram. Soc. 54 (2) 89-93 (1971).

17. P. H. Kubaschewski, E. LL. Evans and C. B. Alcock, "Metallurgical Thermochemistry," Pergamon Press, New York (1967).

18. G. Parravano, "Solid State Reaction Between Magnesium and Chromium Oxides," J. Am. Chem. Soc. 74 6123-25 (1952).

19. P. J. Anderson and P. L. Morgan, "Effects of Water Vapor on Sintering of MgO," Trans. Faraday Soc. 60 930 (1964).

VITA

Gordon Eric Jungquist was born on February 27, 1946, in Jamestown, New York. He received his primary education in Cherry Creek, New York and his secondary education at Pine Valley Central School in South Dayton, New York. He has received his college education from Alfred University, in Alfred, New York, and the University of Missouri-Rolla, in Rolla, Missouri. He received a Bachelor of Science degree in Ceramic Engineering from Alfred University in 1968.

He has been enrolled in the Graduate School of the University of Missouri-Rolla since September 1968 and has held the American Iron and Steel Institute Fellowship for the period September, 1968, to January, 1971.

APPENDICES

APPENDIX A

List of Impurities in Raw Materials

Fisher's Certified MgO

Barium (Ba)	0.004 wt.%	BaO 0.004 wt.%
Iron (Fe)	0.008	Fe_2O_3 0.011
Nitrate (NO_3)	0.005	
Chloride (Cl)	0.005	
Insoluble in dilute HCl	0.020	
Soluble in H_2O	0.30	
Loss on Ignition	1.1	
Ammonium hydroxide ppt.	0.020	
Sulfate and sulfite (as SO_4)	0.003	
Calcium (Ca)	0.03	CaO 0.04
Heavy metals (as Pb)	0.003	PbO 0.003
Manganese (Mn)	0.0003	MnO 0.0003
Potassium (K)	0.003	K_2O 0.004
Sodium (Na)	0.4	N_2O 0.5
Strontium (Sr)	0.002	SrO 0.002

Fisher's Certified Magnesium Nitrate - $Mg(NO_3)_2 \cdot 6H_2O$

Chloride (Cl)	0.0077 wt.%
Iron (Fe)	0.0004
Barium (Ba)	0.002
Sulfate (SO_4)	0.003
Calcium (Ca)	0.002
Insoluble matter	0.002
Phosphate (PO_4)	0.0003
Ammonium (NH_4)	0.003
Heavy metals (as Pb)	0.0003
PH of a 5% solution at 25°C	5.6
Potassium (K)	0.001
Manganese (Mn)	0.0003
Sodium (Na)	0.001
Strontium (Sr)	0.003

Hyperrefiners' Ultra High Pure Chromium Oxide

This chromium oxide was made 99.99% pure by Hyperrefiners by oxidizing ultra high pure chromium.

APPENDIX B

Values of Relative Weight Loss Used to Plot Figure 5

Solid Curve

P_{O_2}	Cr	CrO_3	Total
$1x10^{-13}$	8.4	$7.4x10^{-12}$	8.4
$2x10^{-12}$	8.4	$2.2x10^{-8}$	8.4
9.10^{-12}	2.7	$5.9x10^{-8}$	2.7
$2x10^{-11}$	1.6	$1.2x10^{-7}$	1.6
$2x10^{-10}$	$2.7x10^{-1}$	$5.9x10^{-7}$	$2.7x10^{-1}$
$2x10^{-9}$	$4.2x10^{-2}$	$3.7x10^{-6}$	$4.2x10^{-2}$
$2x10^{-8}$	$8.4x10^{-3}$	$1.8x10^{-5}$	$8.4x10^{-3}$
$2x10^{-6}$	$1.3x10^{-3}$	$1.0x10^{-4}$	$1.4x10^{-3}$
$2x10^{-4}$	$8.4x10^{-6}$	$1.8x10^{-2}$	$1.8x10^{-2}$
$2x10^{-2}$	$2.7x10^{-7}$	$8.1x10^{-1}$	$8.1x10^{-1}$
$2x10^{-1}$	$5.3x10^{-8}$	3.7	3.7
1	$1.5x10^{-8}$	11.7	11.7

Dotted Curve

P_{O_2}	Cr	CrO	CrO_2	CrO_3	Total
$1x10^{-13}$	8.4	--	--	$7.4x10^{-12}$	8.4
$2x10^{-12}$	8.4	--	--	$2.2x10^{-8}$	8.4
$9x10^{-12}$	3.8	$6.2x10^{-1}$	$6.9x10^{-4}$	$5.9x10^{-8}$	4.4
$2x10^{-11}$	2.7	$4.3x10^{-1}$	$7.7x10^{-4}$	$1.2x10^{-7}$	3.1
$2x10^{-10}$	1.1	$1.2x10^{-1}$	$1.4x10^{-3}$	$5.9x10^{-7}$	1.2
$2x10^{-9}$	$4.2x10^{-1}$	$3.1x10^{-2}$	$2.5x10^{-3}$	$3.7x10^{-6}$	$4.5x10^{-1}$
$2x10^{-8}$	$1.5x10^{-1}$	$7.7x10^{-3}$	$4.3x10^{-3}$	$1.8x10^{-5}$	$1.6x10^{-1}$
$2x10^{-6}$	$2.1x10^{-2}$	$5.5x10^{-4}$	$1.6x10^{-2}$	$1.0x10^{-4}$	$3.7x10^{-2}$
$2x10^{-4}$	$2.9x10^{-3}$	$1.5x10^{-4}$	$2.8x10^{-2}$	$1.8x10^{-2}$	$4.9x10^{-2}$
$2x10^{-2}$	$4.2x10^{-4}$	$2.5x10^{-6}$	$1.7x10^{-1}$	$8.1x10^{-1}$	$9.8x10^{-1}$
$2x10^{-1}$	$1.5x10^{-4}$	$6.2x10^{-7}$	$3.1x10^{-1}$	3.7	4.0
1	$8.4x10^{-5}$	$2.5x10^{-7}$	$4.3x10^{-1}$	11.7	12.1